

REVISITING THE GERASIMOVA-ZATSEPIN EFFECT

J.V.R. VAN EIJDEN



Dr. C.J.W.P. Timmermans,
Prof. Dr. S.J. de Jong

July 2015
HEN-482

J.V.R. van Eijden: *Revisiting the Gerasimova-Zatsepin effect, A Monte Carlo simulation*, © July 2015

SUPERVISORS:

Dr. C.J.W.P. Timmermans, Prof. Dr. S.J. de Jong

*I hear and I forget.
I see and I remember.
I do and I understand.*

— Confucius (551BC – 479BC)

CONTENTS

1	INTRODUCTION	1
1.1	The G.Z. effect	1
1.2	The main question	2
1.3	Thesis structure	2
2	INTERACTION PROBABILITY OF COSMIC RAYS WITH PHOTONS FROM THE SUN	3
2.1	Interaction probability	3
2.2	Mean free path	4
2.3	Photon density	5
2.4	Cross section	7
2.5	Results so far	11
3	DEFLECTION OF CHARGED PARTICLES IN THE MAGNETIC FIELD OF THE SUN	17
3.1	Change in direction of the momentum	17
3.2	Program-check	18
3.3	Sun's magnetic fields	20
3.3.1	Dipole field	21
3.3.2	Sunspot field	21
3.3.3	Dynamo field	22
3.3.4	Ring field	22
3.3.5	Total field	22
3.4	Program-check	23
3.5	Ray tracing	24
3.6	Results so far	25
4	INTERACTIONS	27
4.1	Forced interactions	27
4.2	Results so far	28
5	G.Z. FLUX RATE ON EARTH	33
5.1	Slight variation in initial direction	33
5.2	Cosmic ray flux	34
5.3	G.Z. flux rate	35
5.4	Results so far	36
6	DETECTOR CONFIGURATION	39
6.1	Pierre Auger	39
6.2	Results so far	40
6.3	HiSPARC	42
6.4	Results so far	44
7	CONCLUSIONS	47
7.1	The Gerasimova-Zatsepin effect	47
7.2	Current detector setups	47
7.3	Compared with earlier results	47
7.4	What if	48

A APPENDIX A	51
B APPENDIX B	55
C APPENDIX C	57
D APPENDIX D	59
BIBLIOGRAPHY	61

INTRODUCTION

1.1 THE G.Z. EFFECT

N. M. Gerasimova and G. T. Zatsepin [1] described the following effect in 1960:

When a heavy cosmic ray nucleus enters our solar system there is a probability of interacting with a photon from the sun. If the nucleus has a sufficient amount of energy (in the order of EeV¹) it is possible that as a result of the interaction the nucleus radiates off a particle. The two secondaries might hit the Earth and cause two coincident but separate showers.

If both showers are detected it is referred to as a G.Z. event. [Figure 1](#) shows an artist impression of the described phenomenon.

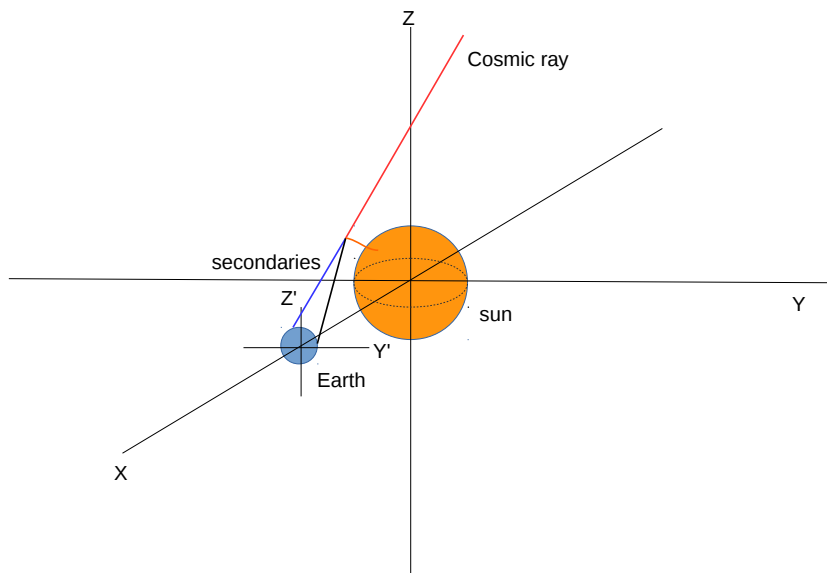


Figure 1: The G.Z. effect

¹ EeV: Exaelectronvolt = 10^{18} electronvolt = 0.16 J

1.2 THE MAIN QUESTION

What is the rate of G.Z. events on Earth and how can they be detected?

This master thesis focuses on answering this question by developing a detailed model and associated Monte Carlo simulation. This main question is divided into sub-questions:

1. *What is the rate of coincident showers due to the G.Z. effect?*
2. *What is the distance between those coincident showers?*
3. *What is the relation between rate and distance between the shower and the distance between the primary trajectory and the sun?*
4. *Is it possible to measure this effect with the Pierre Auger observatory or HiSPARC?*

If it is possible to measure the G.Z. effect it might be used as a tool to measure the fraction of heavy nuclei in cosmic rays. Up until now there are no publications of measurements of the G.Z. effect. Several theoretical studies have been performed [2, 3, 4, 5, 6, 7].

1.3 THESIS STRUCTURE

Several steps were performed in order to create a detailed model and associated Monte Carlo simulation. The structure of this thesis reflects the individual steps, which are:

1. Calculate the interaction probability of a heavy cosmic ray nucleus with a photon from the sun.
2. Implement the deflection of a heavy cosmic ray nucleus along its path due to the Solar magnetic field.
3. Generate interactions and track the secondaries.
4. Calculate the flux rate on Earth.
5. Implement detector configurations.

The model was checked frequently on correct functionality. Only the important "Program-checks" are mentioned in a separate paragraph. Each chapter ends with a paragraph "Results so far". This paragraph describes the results of different calculations done with the theory covered in the preceding chapter. Based on these results preliminary conclusions are drawn.

2

INTERACTION PROBABILITY OF COSMIC RAYS WITH PHOTONS FROM THE SUN

In this chapter the probability of an interaction between a heavy cosmic ray nucleus with a photon from the sun is calculated. The possible G.Z. events that reach the Earth are of interest, therefore the total probability is calculated only for a path aimed towards the Earth. [Figure 2](#) shows an artist impression of such a trajectory. This figure shows the sun in the center, and the position of the Earth on the x-axis of the chosen coordinate system.

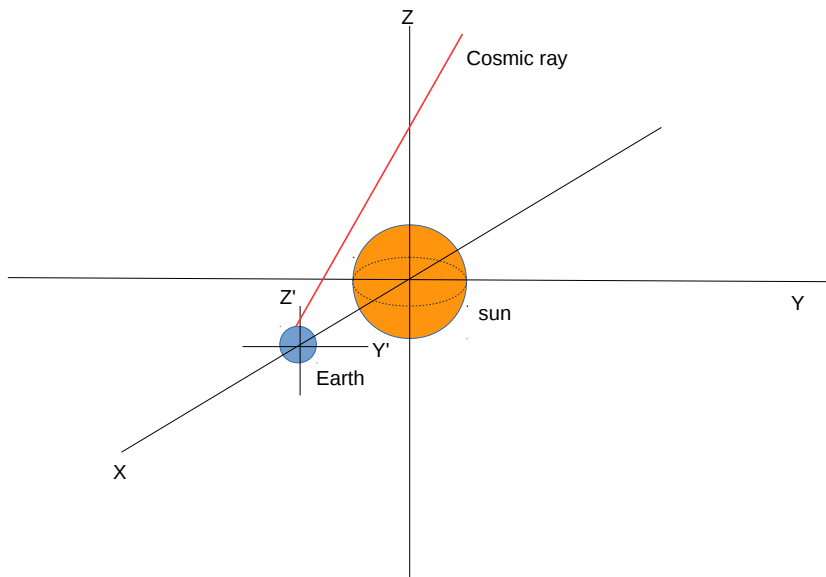


Figure 2: Cosmic ray trajectory

2.1 INTERACTION PROBABILITY

The trajectory of the nucleus is divided into i steps. In each step the particle travels a distance $dr = \sqrt{dx^2 + dy^2 + dz^2}$. The probability for an interaction to occur up to step i is calculated by performing a Riemann summation

$$P_i = \sum_x \sum_{\epsilon} (1 - P_{i-1}) \cdot \left(\frac{1}{\lambda} e^{-x_i/\lambda} \cdot d\epsilon \cdot dr \right), \quad (1)$$

with

- P_i interaction probability up to step i ,
- λ the mean free path of the nucleus (km), which depends on the photon energy, see section 1.1.1,
- x_i the sum of dr , the distance traveled by the nucleus (km) up to step i ,
- $d\epsilon$ the photon energy, which is integrated over for each step, and
- dr the distance (km) traveled in step i .

For reasons covered later in this chapter the calculation of the trajectory starts from a distance of 4 Astronomical Units (AU, distance Sun-Earth). Therefore the particle might travel up to 5 AU before reaching the Earth. In order to make efficient use of the CPU-time dx can be quite large. The summation is made slightly more accurate by calculating the interaction probability at $\bar{x} = x_{i-1} + 0.5 \cdot dr$. Furthermore the step size dr is set as a function of the distance between the nucleus and the sun and as a function of the distance between the nucleus and Earth. The accuracy is increased by decreasing the step size close to the sun. The step size is also decreased close to Earth. By doing so a more accurate image of the particle distribution on the surface of the Earth can be obtained.

2.2 MEAN FREE PATH

The average distance that a nucleus can travel before it interacts with a photon is called the mean free path. The mean free path can be calculated using

$$\lambda = \left(\frac{dn}{d\epsilon} \cdot \sigma \right)^{-1}, \quad (2)$$

with

- $\frac{dn}{d\epsilon}$ the photon density defined as the number of photons of a certain energy per volume at a distance from the sun, the derivation of this function is covered in [Section 2.3](#), and
- σ the cross section that depends on the energy in the center of mass frame of the collision, ϵ^* . This parameter is discussed in [Section 2.4](#).

2.3 PHOTON DENSITY

Photons are energy packets radiated by objects. To be able to calculate the photon density at a certain point in our solar system it is necessary to understand the energy radiation of the sun. Therefore, this section has two paragraphs. The first describes the radiation of energy and the second the radiation of photons from the sun.

Planck's formula [8] describes the radiation density inside a black body

$$d\epsilon(\nu, T) = \frac{8\pi h\nu^3}{c^3} \frac{1}{e^{h\nu/k_B T} - 1} d\nu. \quad (3)$$

The outward emitted radiation per square meter is obtained by multiplying by $c/4$,¹ hence the energy flux density as a function of frequency ν from the surface of the sun is given by

$$d\Phi(\nu, T) = \frac{2\pi h\nu^3}{c^2} \frac{1}{e^{h\nu/k_B T} - 1} d\nu, \quad (4)$$

with

Φ power per square meter at the sun's surface in $\left[\frac{\text{J}}{\text{m}^2\text{s}}\right]$,

ν frequency in Hertz,

T temperature in Kelvin,

h Planck's constant, $6.626 \cdot 10^{-34} \text{ J} \cdot \text{s}$,

k_B Boltzmann's constant, $1.380 \cdot 10^{-23} \text{ J} \cdot \text{K}^{-1}$, and

c speed of light, $3.00 \cdot 10^8 \text{ m/s}$.

The measured solar constant is $\Phi_{\text{Earth}}^{\text{Observed}} = 1.36 \text{ kW/m}^2$ [12].

The radiation emitted at the surface of the sun is given by

$$\Phi_{\text{SUN}} = \Phi_{\text{Earth}}^{\text{Observed}} \cdot \frac{d_{\text{AU}}^2}{r_{\text{eff.sun}}^2} \quad (5)$$

where

d_{AU} is the distance earth, sun, one Astronomical Unit (AU), and

$r_{\text{eff.sun}}$ the effective radius of the sun.

The total radiation of the sun is found to be

$$\Phi_{\text{SUN}} = 1.36 \cdot (215.09)^2 = 6.29 \cdot 10^7 \text{ kW/m}^2. \quad (6)$$

With this and the use of Stefan-Boltzmann law [9, 10], see for a derivation [Appendix A](#), the effective temperature of the photosphere is

¹ The fraction of the radiation traveling with the speed of light in direction θ, ϕ is $(c \cos \theta / 4\pi) d\Omega$, using Lambert's cosine law for radiation intensity [11]. For the fraction of radiation from a surface moving outwards, Ω has to be integrated over the half sphere, giving $\int_{\phi=0}^{2\pi} \int_{\theta=0}^{\pi/2} (c \cos \theta / 4\pi) d\phi d\cos \theta = c/4$.

$$T = \sqrt[4]{\frac{\Phi}{\sigma}} = \sqrt[4]{\frac{6.29 \cdot 10^7}{5.67 \cdot 10^{-8}}} = 5771 \text{ K}, \quad (7)$$

with

$$\sigma \text{ Stefan-Boltzmann's constant } \frac{2\pi^5 k^4}{15 h^3 c^2} = 5.67 \cdot 10^{-8} \text{ Js}^{-1} \text{ m}^{-2} \text{ K}^{-4}.$$

To be able to calculate the photon density, the number of photons emitted by the sun is of interest. So [Equation 4](#) can be rewritten as a function of the photon energy, $\epsilon = h \cdot v$,

$$d\Phi(\epsilon, T) = \frac{2\pi\epsilon^3}{c^2 h^2} \frac{1}{e^{\epsilon/k_B T} - 1} d\epsilon \cdot \frac{1}{h}. \quad (8)$$

Note that the additional factor $\frac{1}{h}$ comes from the change in derivative. The number of photons of a certain energy emitted per square meter per second from the surface of the sun is given by

$$dn(\epsilon, T) = \frac{2\pi}{c^2 h^3} \frac{\epsilon^2}{e^{\epsilon/k_B T} - 1} d\epsilon. \quad (9)$$

This number will reduce with $\frac{1}{r^2}$ outside of the sun. The simulation uses Astronomical Units (AU); $r = \frac{1 \text{ AU}}{r_\odot}$.² The photon density at a certain distance from the sun ($r > r_\odot$) is given by

$$dn(\epsilon, T, r_{\text{AU}}) = \left(\frac{r_\odot}{1 \text{ AU}}\right)^2 \cdot \left(\frac{1}{r_{\text{AU}}}\right)^2 \cdot \frac{2\pi}{c^2 h^3} \frac{\epsilon^2}{e^{\epsilon/k_B T} - 1} d\epsilon. \quad (10)$$

The next step is to calculate the number of photons per volume. In one second the photons travel a distance of $c = 3.00 \cdot 10^8 \text{ m}$. So if [Equation 10](#) is divided by c , it provides us with the number of photons per unit of volume

$$d\rho(\epsilon, T, r_{\text{AU}}) = \left(\frac{r_\odot}{1 \text{ AU}}\right)^2 \cdot \left(\frac{1}{r_{\text{AU}}}\right)^2 \cdot \frac{2\pi}{c^3 h^3} \frac{\epsilon^2}{e^{\epsilon/k_B T} - 1} d\epsilon. \quad (11)$$

Next, all constants of [Equation 11](#) are combined into a single scaling factor. For this the unit system J and m^3 is changed to eV and cm^3

$$d\rho(\epsilon, r_{\text{AU}}) = 7.13 \cdot 10^7 \cdot \left(\frac{1}{r_{\text{AU}}}\right)^2 \cdot \frac{\epsilon^2}{e^{\epsilon/0.497} - 1} d\epsilon, \quad (12)$$

$d\rho$ the number of photons of energy ϵ per cm^3 per eV,

ϵ the photon energy in eV, and

r_{AU} the distance from the sun in astronomical units.

Note that $7.13 \cdot 10^7 \text{ cm}^{-3}$ is in agreement with [2, 3, 4, 5]. In these articles this number was derived as a normalization factor to reproduce the correct photon flux as measured in experiments. In [Figure 3](#), [Equation 12](#) is plotted at a distance of 1AU. Note that the peak in the photon density is at an energy of 0.79 eV. This energy is independent of the distance to the sun.

² The large photon density near the sun is one of the reasons why the step size dl , covered in [Section 2.1](#), will be varied as a function of the distance between the nucleus and the sun.

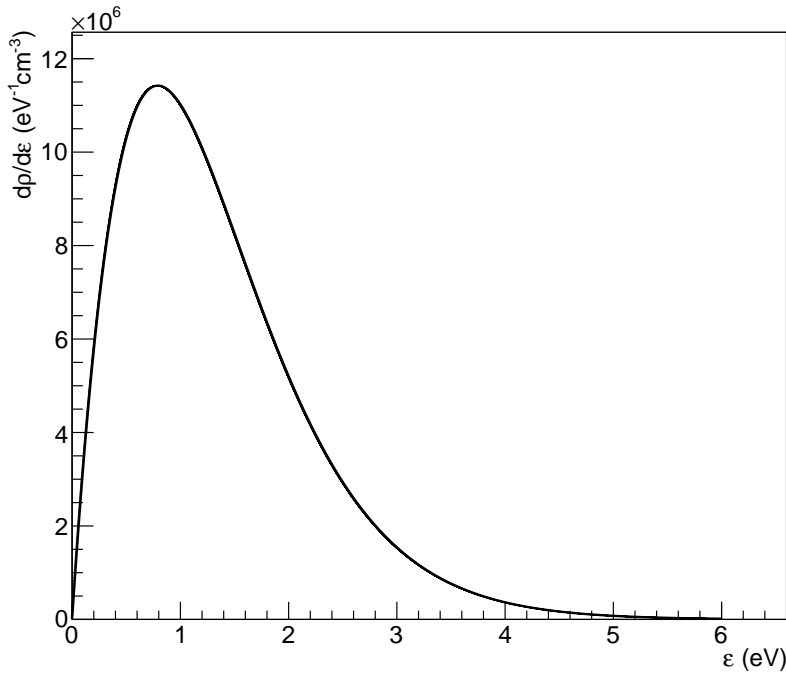


Figure 3: The density of solar photons according to [Equation 12](#) evaluated at $r_{AU} = 1$. The peak value is $\frac{d\rho}{d\epsilon} = 1.14 \cdot 10^7 eV^{-1} cm^{-3}$ at a photon energy of $\epsilon = 0.79$ eV. The effective temperature of the photosphere is taken $T = 5771$ K.

2.4 CROSS SECTION

In calculating the cross section for a photon with a nucleus special relativity plays an important role. From the rest frame of the nucleus the photons appear to be gamma rays. In the rest frame of the Earth (for convenience also the rest frame of the sun) we see both particles moving. To implement this properly the first paragraph describes the cross section in the rest frame of the nucleus. The second paragraph describes the Lorentz transformation towards the rest frame of the sun.

The cross section for an interaction between a nucleus and a photon from the sun depends on the energy in the center of mass frame of the collision. Experiments show that at certain energies there are resonance peaks in this cross section. For this thesis, the most important

resonance peak is the 'Giant Dipole Resonance'.

The cross section is parametrised according to [13] and [14]³

$$\sigma_i(\epsilon^*) = \begin{cases} 0, & \epsilon^* < \epsilon_{\text{thr}}, \\ \xi_i \Sigma_d W_i^{-1} \exp\left(\frac{-2(\epsilon^* - \epsilon_{p,i})^2}{\Delta_i^2}\right) \times \\ & \Theta_+(\epsilon_{\text{thr}})\Theta_-(\epsilon_1), & \epsilon_{\text{thr}} \leq \epsilon^* \leq \epsilon_1, \\ \frac{\zeta \Sigma_d \Theta_+(\epsilon_{\text{max}})\Theta_-(\epsilon_1)}{\epsilon_{\text{max}} - \epsilon_1}, & \epsilon_1 < \epsilon^* \leq \epsilon_{\text{max}}, \\ 0, & \epsilon^* > \epsilon_{\text{max}}. \end{cases} \quad (13)$$

The resonant part ($\epsilon_{\text{thr}} \leq \epsilon^* \leq \epsilon_1$) is based on the Thomas-Reiche-Kuhn sum rule for the photoabsorption cross section

$$\Sigma_d = \int_0^\infty \sigma(\epsilon) d\epsilon = \frac{2\pi^2 e^2 \hbar}{MC} \frac{NZ}{A} = 60 \frac{NZ}{A} [\text{mb} - \text{MeV}]. \quad (14)$$

Furthermore

$\sigma_i(\epsilon^*)$	is the cross section for a certain nucleus as a function of ϵ^* in cm^2 ,
ϵ^*	the energy of the photon in the rest frame of the nucleus,
A	number of nucleons in the nucleus,
Z	the number of protons in the nucleus,
N	$N=A-Z$, number of neutrons in the nucleus,
$\Theta_+(x), \Theta_-(x)$	Heaviside step functions,
W_i	a normalization constant $W_i = \Delta_i \sqrt{\frac{\pi}{8}} \left[\text{erf}\left(\frac{\epsilon_{\text{max}} - \epsilon_{p,i}}{\Delta_i/\sqrt{2}}\right) + \text{erf}\left(\frac{\epsilon_{p,i} - \epsilon_1}{\Delta_i/\sqrt{2}}\right) \right]$,
Δ_i	Width of the resonance, MeV, see [14],
$\epsilon_{p,i}$	peak energy, MeV, see [14],
ξ_i, ζ	dimensionless integrated cross sections [14], and
$\epsilon_{\text{thr}}, \epsilon_1, \epsilon_{\text{max}}$	different energy ranges in MeV see [13].

For a single proton loss ($i = 1$) due to an interaction with a photon (γ, p) the different constants for Fe-56 and O-16 are given in Table 1 [13, 14].

³ The formula of Stecker and Puget is faithfully reproduced. It is not clear why the factor two in the exponent is in the numerator and not in the denominator. It might be a mistake in their article, or the width is meant to approximate the FWHM (Full Width at Half Maximum), in which case the scaling by factor 4 is only a very rough approximation of 2.355^2 .

Z	A	ϵ_{thr} (MeV)	ϵ_1 (MeV)	ϵ_{max} (MeV)	Δ_1 (MeV)	$\epsilon_{p,1}$ (MeV)	ξ_1	ζ
26	56	10.2	18 (27)	150	8	18	0.98	0.95
8	16	12.1	24 (33)	150	9	24	0.83	1.10

Table 1: Parameters describing the cross section parameterization of [Equation 13](#).

In [Figure 4](#) the cross sections for Fe-56 and O-16 are shown. Note that the maximal values are obtained at photon energies of respectively $1.8 \cdot 10^7$ eV and $2.4 \cdot 10^7$ eV. The sudden cutoff at 10.2 MeV for iron and 12.1 MeV for oxygen results from the threshold energy ϵ_{thr} of the cross section parametrization. For the upper limit of the resonance region (ϵ_1) a floating transition is created. Therefore the resonance peak matches ‘nicely’ with the plateau that extends up to ϵ_{max} . [Table 1](#) above shows the ϵ_1 energies that were used here in brackets. These are higher than the values found in the references.

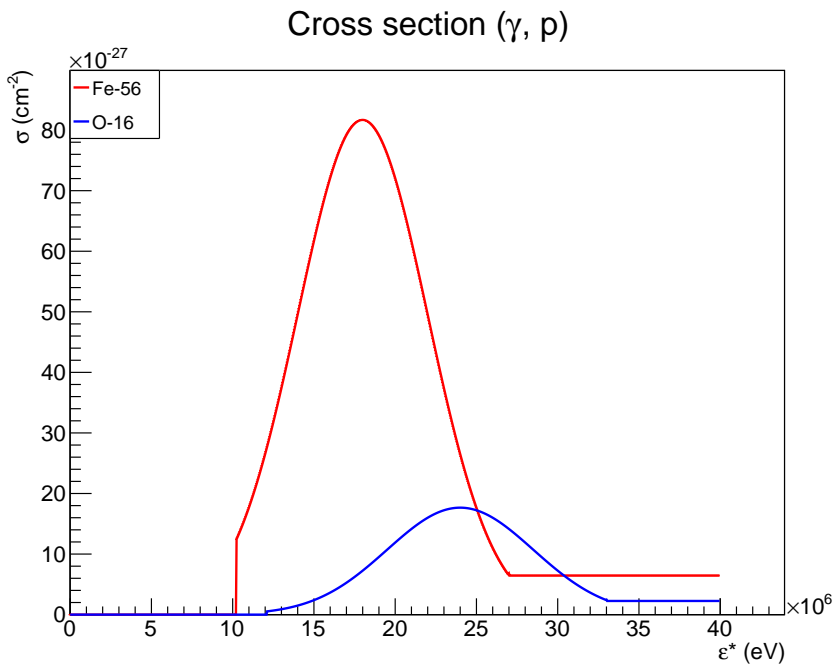


Figure 4: Photon nucleus cross section of the Giant Dipole Resonances as a function of the photon energy in the rest frame of the nucleus. The cross sections for iron and oxygen primaries are shown in red and blue respectively.

	$\sigma(\text{cm}^{-2})$	$\epsilon^*(\text{eV})$
Fe-56	$8.2 \cdot 10^{-26}$	$1.8 \cdot 10^7$
O-16	$1.8 \cdot 10^{-26}$	$2.4 \cdot 10^7$

Table 2: Maximum cross sections in [Figure 4](#).

The photon energy in the rest frame of the nucleus (ϵ^*) can be obtained using,

$$\epsilon^* = \frac{\epsilon \sqrt{P_N^2 + m_N^2} - \epsilon P_N \cos \alpha}{m_N}, \quad (15)$$

with

- ϵ^* photon energy in the rest frame of the nucleus, in eV,
- ϵ photon energy in the restframe of the sun, in eV,
- P_N momentum of the particle in eV,
- m_N mass of the particle in eV, and
- α angle between photon and nucleus.

For the derivation of this relation see [Appendix B](#).

To calculate the interaction probability between the nucleus and a photon, at each point in space the angle between the two is calculated assuming the photons from the sun travel in straight lines from its center. The cross section plots for a head-on collision of Fe-56 and O-16 with a photon from the sun, as a function of the cosmic ray momentum are shown in [Figure 5](#). A photon energy in the rest frame of the sun of $\epsilon = 0.79$ eV is used. This corresponds to the maximum in the radiated photon density. The peak in [Figure 5](#) will shift if a different angle between photon and nucleus is considered, as listed in [Table 3](#).

	α	$\sigma(\cdot 10^{-26} \text{cm}^{-2})$	$\epsilon^*(\text{EeV})$
Fe-56	π	8.2	0.59
	0.5π	8.2	1.2
O-16	π	1.8	0.23
	0.5π	1.8	0.45

Table 3: Maximum cross sections in [Figure 5](#).

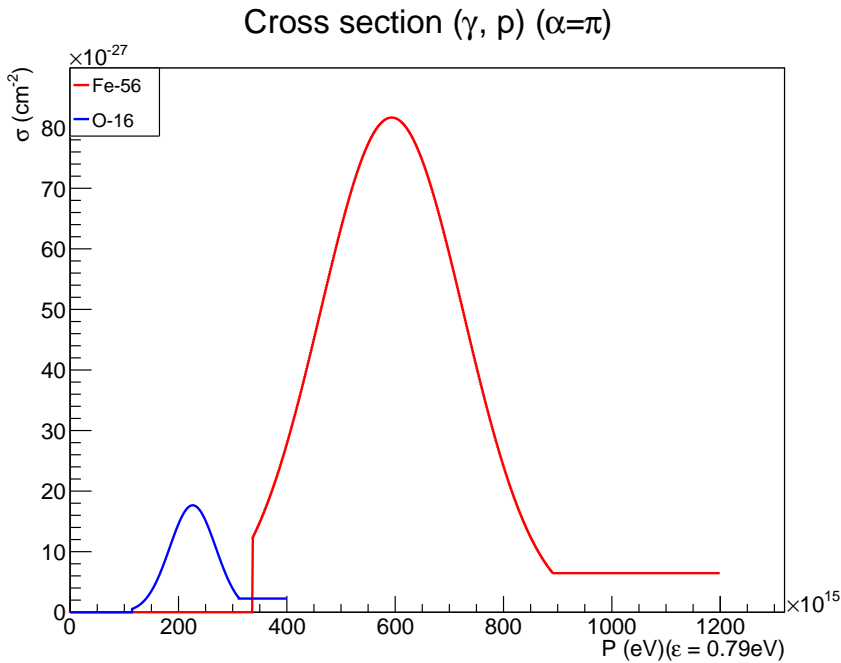


Figure 5: Photon nucleus cross section of the Giant Dipole Resonances as a function of the nucleus energy in the rest frame of the sun. The red curve to the right is for Iron nuclei and the blue curve to the left is for incident Oxygen nuclei.

2.5 RESULTS SO FAR

With the knowledge described in the previous paragraphs the interaction probability is calculated for two different configurations. Particles are shot towards the Earth from a point at a distance of 4 AU from the center of the sun. These points lie on a circle in the xy-plane and the yz-plane as illustrated in [Figure 6](#) and [Figure 7](#).

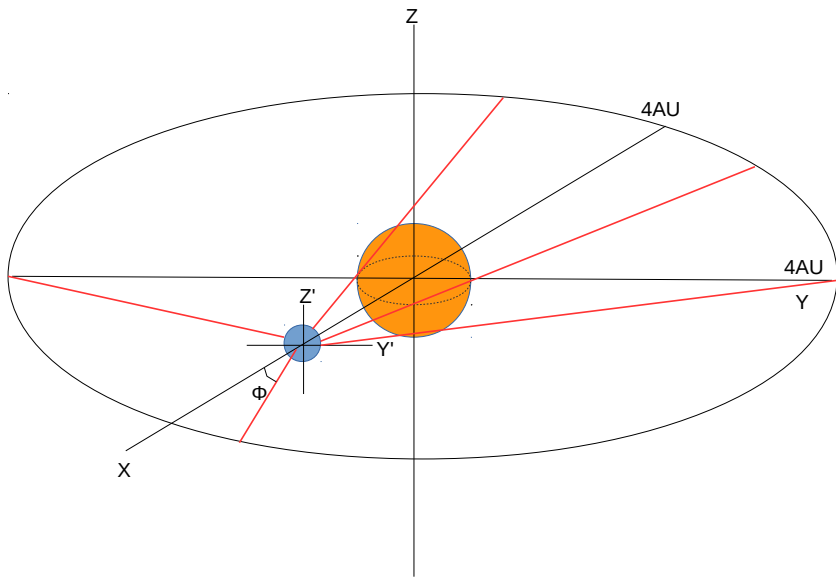


Figure 6: Various cosmic ray paths from a 4 AU radius sphere around the sun to the Earth in the $x - y$ plane.

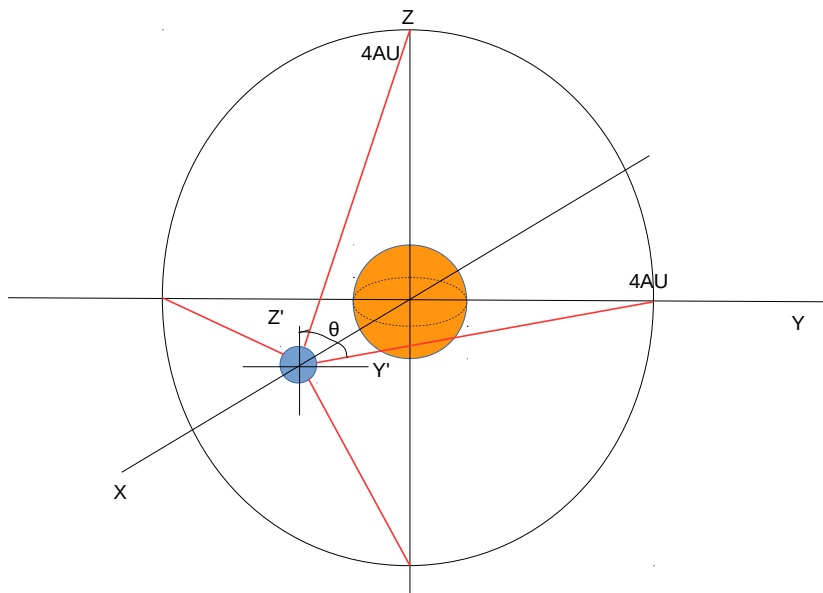


Figure 7: Various cosmic ray paths from a 4 AU radius sphere around the sun to the Earth in the $y - z$ plane.

Along each trajectory at each step the interaction probability is calculated by summing (integrating) over photon energies in the rest frame of the sun from 0.04 eV to 24.0 eV. The probabilities at each step are summed until the particle hits the Earth. This results in a total probability as a function of the direction of observation; ϕ for the xy-plane and θ for the yz-plane. These integral probabilities are shown in [Figure 8](#) and [Figure 9](#). Note that due to collisions with the sun there are no entries around $\phi/\pi = 1$, the peak is cut off instead of a dip to zero.

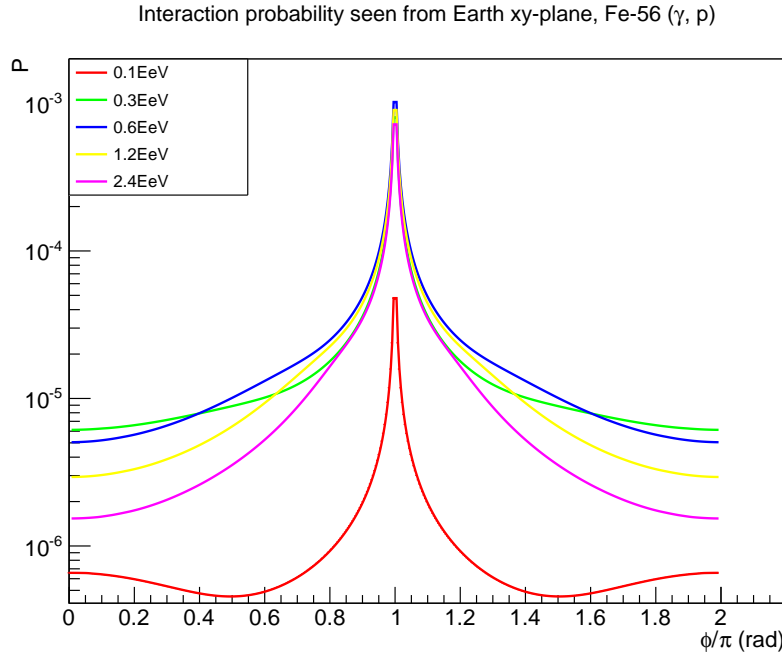


Figure 8: Interaction probability for Iron with photons from the sun as a function of the angle in the Earth-sun plane with respect to the direction of the sun to the Earth, ϕ . The sun is seen at $\phi/\pi = 1$ from the Earth. The different curves correspond to different nucleon energies in the rest frame of the sun.

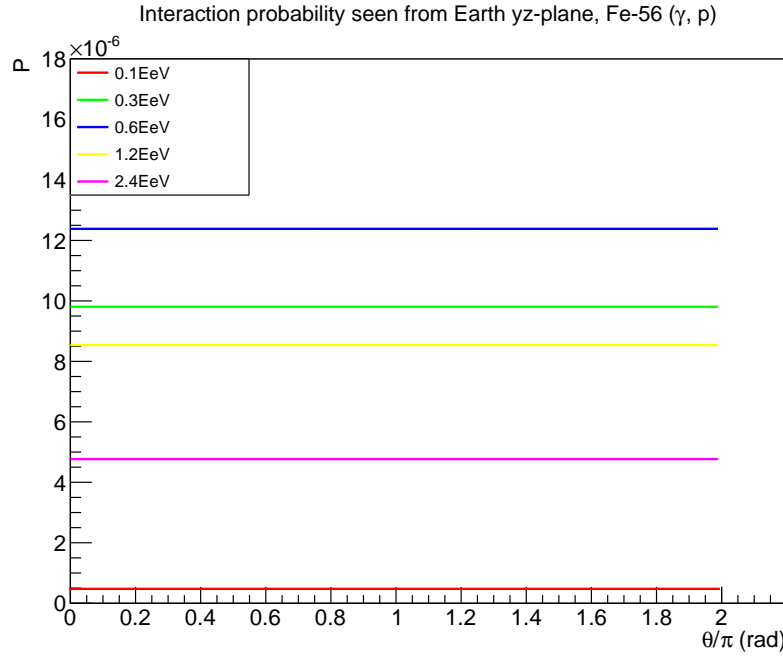


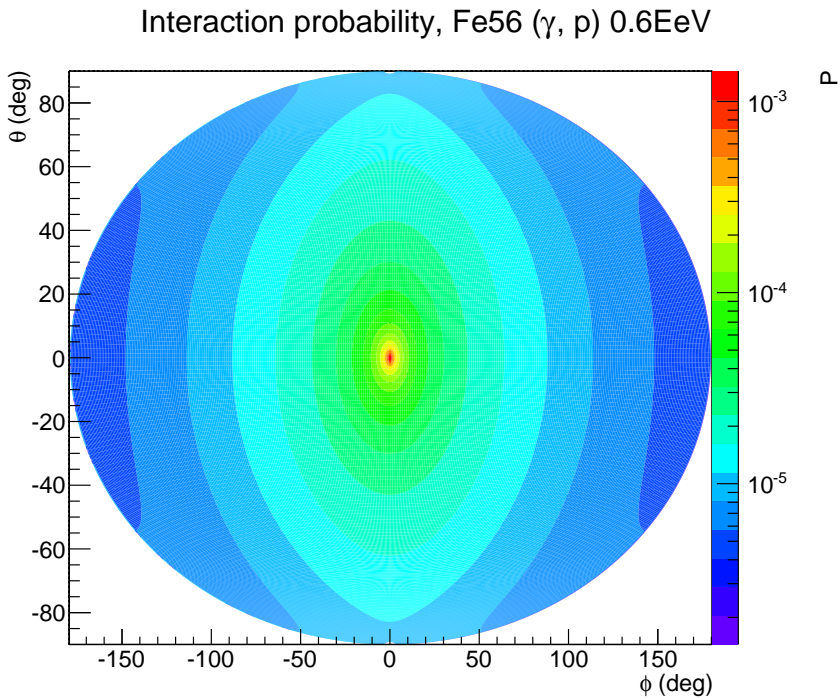
Figure 9: Interaction probability for Iron nuclei with photons from the sun as a function of the angle θ as defined in Figure 7. The different curves correspond to different nucleon energies in the rest frame of the sun.

Figure 8 shows that the interaction probability is a mix between the photon density function on the one hand and the collision angle on the other. At least two important conclusions can be drawn from this result:

1. The highest interaction probability is obtained for an iron nucleus traveling near the sun with an energy of 0.6 EeV. This is in agreement with the position of the peak in the plot of the cross section at an angle between the photon and nucleus of $\alpha = \pi$, see Figure 5 for a photon energy of $\epsilon = 0.79$ eV, which was obtained from Figure 3.
2. For an iron nucleus with an energy of 0.1 EeV the interaction probability increases slightly when it arrives at a direction near 0 radians. This effect is due to the head-on collision of the nucleus with the photons. The photon energy in the rest frame of the nucleus depends on the cosine of the angle between the photon and the nucleus. At $\alpha = 0$ and $\alpha = 2\pi$ radians the cross section and therefore the interaction probability is increased.

[Figure 9](#) shows that there is no theta dependence for the chosen phi angle.

Finally, a projection of the interaction probability for the entire sky as seen from the Earth is made. This is calculated in steps of one degree. In [Figure 10](#) and [Figure 11](#) a transformation in the definition of ϕ and θ is made in order to accommodate to the Aitoff projection provided by the Root programme. The sun is now located in the center at $(0,0)$. [Figure 11](#) is in agreement with the line of 0.1 EeV in [Figure 8](#). We see a slight increase in interaction probability when we look away from the sun.



[Figure 10](#): Sky projection of the interaction probability, in color code, of an Iron nucleus of energy 0.6 EeV in the rest frame of the sun travelling from a 4 AU sphere around the sun to the Earth.

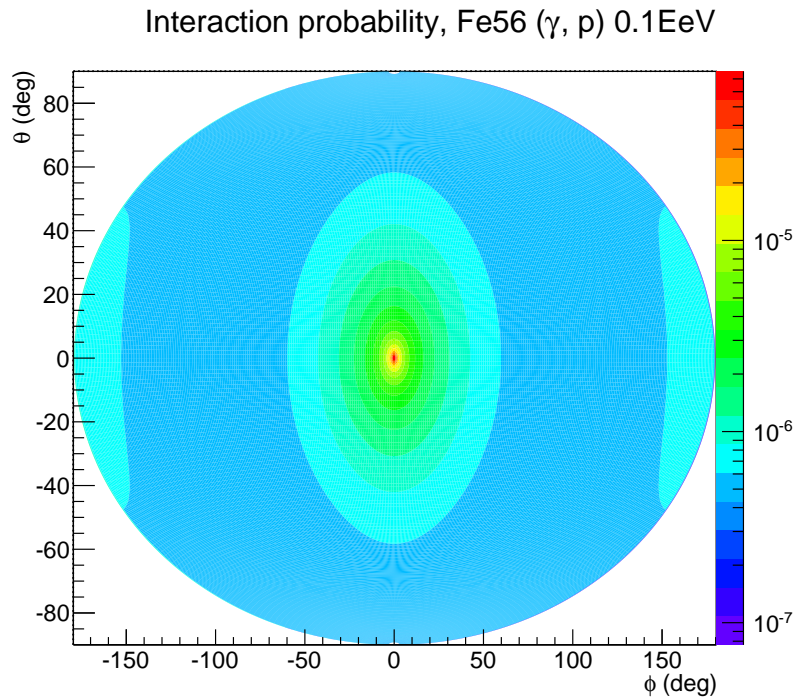


Figure 11: Sky projection of the interaction probability, in color code, of an Iron nucleus of energy 0.1 EeV in the rest frame of the sun traveling from a 4 AU sphere around the sun to the Earth.

3

DEFLECTION OF CHARGED PARTICLES IN THE MAGNETIC FIELD OF THE SUN

Due to the interstellar magnetic field the nucleus doesn't follow a straight line as assumed in [Chapter 2](#). The distance traveled in each step, dl as mentioned in [Equation 1](#), changes in each dimension proportionally to the change in momentum in that direction.

3.1 CHANGE IN DIRECTION OF THE MOMENTUM

Due to the magnetic fields of the sun the direction of momentum of the traveling particle changes along its path. This is calculated with

$$d\vec{P} = \frac{Z \cdot c}{P} \cdot (\vec{P} \times \vec{B}) ds, \quad (16)$$

with

- $d\vec{P}$ the change in momentum of the particle in the x , y and z direction in eV,
 - Z number of charged particles (protons) in the nucleus,
 - c speed of light in m/s,
 - P total momentum of the particle in eV,
 - $\vec{P} \times \vec{B}$ cross product of momentum in eV and magnetic field in T,
 - ds distance traveled by the particle in m, and
- Note! The unit of Tesla is $[\frac{\text{eV}\cdot\text{s}}{\text{m}^2}]$ therefore ds and c must be in [m] and [m/s].

For a derivation, see [Appendix C](#).

3.2 PROGRAM-CHECK

[Equation 16](#) is implemented in a program. To check if the program works correctly the next formula is used

$$r[\text{AU}] = \frac{1}{4.5 \cdot 10^{19}} \cdot \frac{P}{Z \cdot B}, \quad (17)$$

where

$r[\text{AU}]$ radius of curvature in AU,

P momentum in eV,

Z number of charged particles, and

B magnetic field in Tesla.

For the derivation of this formula, see [Appendix D](#).

For example a Fe-56 particle with a momentum of $P = 6.0 \cdot 10^{17}$ eV travels perpendicular to a magnetic field $B=10^{-5}$ T over a distance of 5.0 AU. The radius of curvature is (see [Equation 17](#))

$$r[\text{AU}] = 51.3 \text{ AU}.$$

The deflection in one dimension over 5.0 AU is then

$$h = 51.3 - \sqrt{51.3^2 - 5^2} = 0.24 \text{ AU}.$$

The start values for the program are

$$\vec{P} = \begin{Bmatrix} 6.0 \cdot 10^{17} \text{ eV} \\ 0 \text{ eV} \\ 0 \text{ eV} \end{Bmatrix}, \quad \vec{x} = \begin{Bmatrix} -4.0 \text{ AU} \\ 0 \\ 1.1 \cdot r_{\odot} \end{Bmatrix}, \quad \vec{B} = \begin{Bmatrix} 0 \text{ T} \\ 0 \text{ T} \\ 10^{-5} \text{ T} \end{Bmatrix}.$$

[Figure 12](#) shows that the program calculates properly the deflection for this simple example.

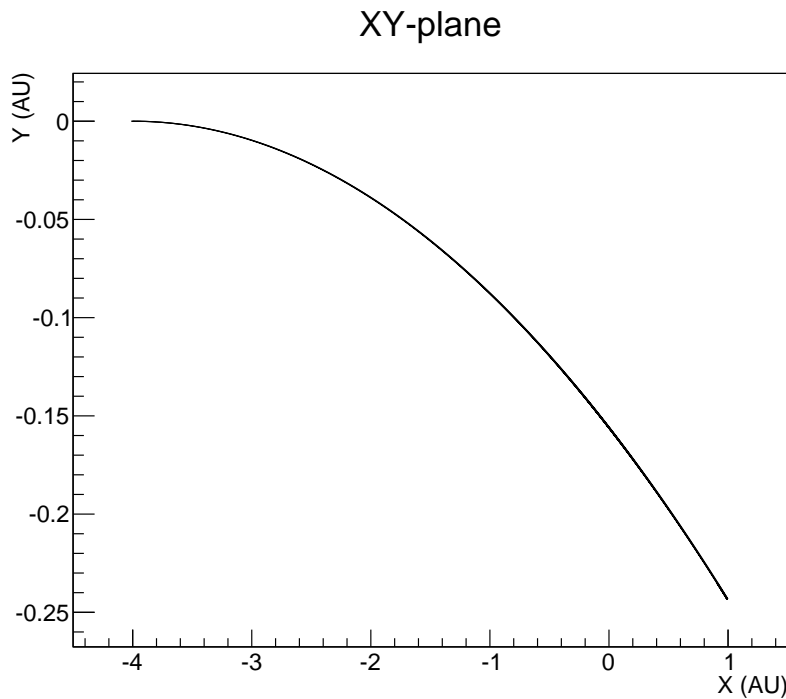


Figure 12: Calculated trajectory of an iron nucleus of $6.0 \cdot 10^{17}$ eV in a homogeneous magnetic field of $B = 10^{-5}$ T traveling from 4 AU behind the sun to the Earth at 1 AU in front of the sun. The magnetic field is perpendicular to the $x - y$ plane in which the trajectory is shown. The deflection from a straight path over the 5 AU traveled is 0.24 AU in accordance with the simple estimate made in the text.

3.3 SUN'S MAGNETIC FIELDS

The model used to describe the magnetic field of the sun [5] [15] is written in cylindrical coordinates (z, ρ, ϕ) . In the simulation a conversion to Cartesian coordinates is made. [Figure 13](#) is an artist impression of the four different magnetic field components used in this thesis.

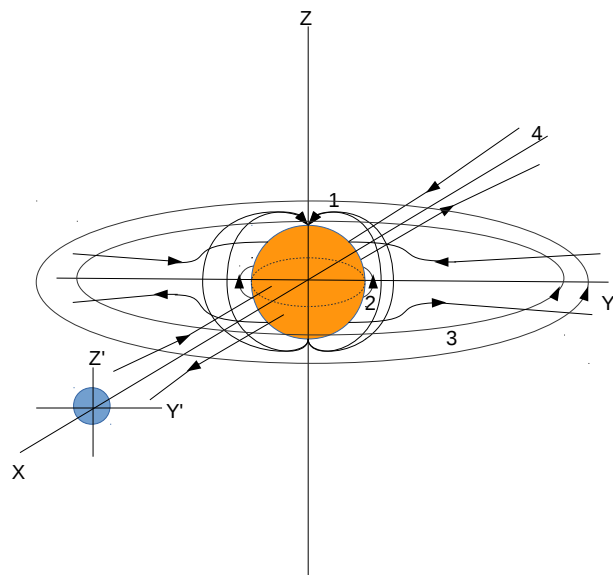


Figure 13: Artist impression of magnetic field components around the sun. The dipole field is marked as 1; the sun spot field as 2; the dynamo field as 3; and the ring field as 4. These components are discussed in the text.

3.3.1 Dipole field

The dipole field is marked as 1 in [Figure 13](#) and modelled as follows

$$B_z^{\text{dip}} = -\left(\frac{B_s r_1^3}{2}\right) (2z^2 - \rho^2) (z^2 + \rho^2)^{-5/2}, \quad (18)$$

$$B_\rho^{\text{dip}} = -\left(\frac{3B_s r_1^3}{2}\right) \rho z (z^2 + \rho^2)^{-5/2}, \quad (19)$$

$$B_\phi^{\text{dip}} = 0, \quad (20)$$

where

$$B_s = 2 \cdot 10^{-4} \text{ T},$$

$$r_1 = r_\odot \text{ (radius of the sun), and}$$

$$\rho = \sqrt{x^2 + y^2}.$$

In the simulation r_1 is rescaled to 1. So the coordinates z , ρ and ϕ in the functions above are provided in units of r_\odot

3.3.2 Sunspot field

The field due to the sunspots is marked as 2 in [Figure 13](#) and modelled by 180 dipoles placed around the equator of the sun. [Equation 18](#), [Equation 19](#) and [Equation 20](#) are used to describe each of these dipoles. However, different values are used for the parameter

$$B_s = 0.1 \text{ T, and}$$

$$r_1 = 0.1 r_\odot.$$

The dipoles are placed at a distance from the center of the sun of $0.8r_\odot$. Therefore, only part of the field lines appear outside of the sun. To calculate the field strength at a point in space the distance to each individual dipole is calculated and the individual field components are added.

3.3.3 *Dynamo field*

This field is marked as 3 in [Figure 13](#). Processes in the photosphere of the sun are responsible for this part of the field. The resulting circular field only has a ϕ direction.

$$B_\phi^{\text{dyn}} = \text{sign}(z) B_{\phi 0} \frac{\rho_0}{\rho}, \quad r_1 < \sqrt{z^2 + \rho^2} < r_2, \quad (21)$$

with

$$B_{\phi 0} = 3.5 \cdot 10^{-9} \text{ T},$$

$$\rho_0 = 1.0 \text{ AU, and}$$

$$\rho = \sqrt{x^2 + y^2}.$$

Note that

$$\sqrt{z^2 + \rho^2} = r,$$

$$r_1 = r_\odot, \text{ and}$$

$$r_2 = 4.0 \cdot \text{AU} \text{ (in the simulation)}.$$

3.3.4 *Ring field*

The solar wind can be seen as a current generating a ring field. This field is marked as 4 in [Figure 13](#) and can be modelled with

$$B_z^{\text{ring}} \simeq B_{\rho 0} \rho_0^2 |z| (z^2 + \rho^2)^{-3/2}, \quad (22)$$

$$B_\rho^{\text{ring}} \simeq \text{sign}(z) B_{\rho 0} \rho_0^2 \rho (z^2 + \rho^2)^{-3/2}, \quad (23)$$

with

$$B_{\rho 0} = -3.5 \cdot 10^{-9} \text{ T, and}$$

$$\rho_0 = 1.0 \text{ AU}.$$

3.3.5 *Total field*

The total field is the sum of the individual field strengths at that specific point in space

$$\vec{B}_{\text{total}} = \vec{B}^{\text{dip}} + \vec{B}^{\text{spot}} + \vec{B}^{\text{dyn}} + \vec{B}^{\text{ring}}. \quad (24)$$

3.4 PROGRAM-CHECK

The magnetic field of the sun at the Earth, $r=1.0$ AU, is given by

$$\vec{B} = \begin{Bmatrix} -3.5 \cdot 10^{-9} \text{ T} \\ 3.5 \cdot 10^{-9} \text{ T} \\ 1.8 \cdot 10^{-9} \text{ T} \end{Bmatrix}, \quad B_{\text{total}} = 5.3 \cdot 10^{-9} \text{ T}.$$

This model provides a relatively high magnetic field strength for a period of normal solar activity (~ 2 to ~ 5 nT). [16]

In [Figure 14](#) and [Figure 15](#) color plots of the total magnetic field around the sun are shown in two different planes. Note that the axes are in units of the radius of the sun. Also note the difference in color range indicating the field strength. The z -component of the magnetic field is by far the strongest component.

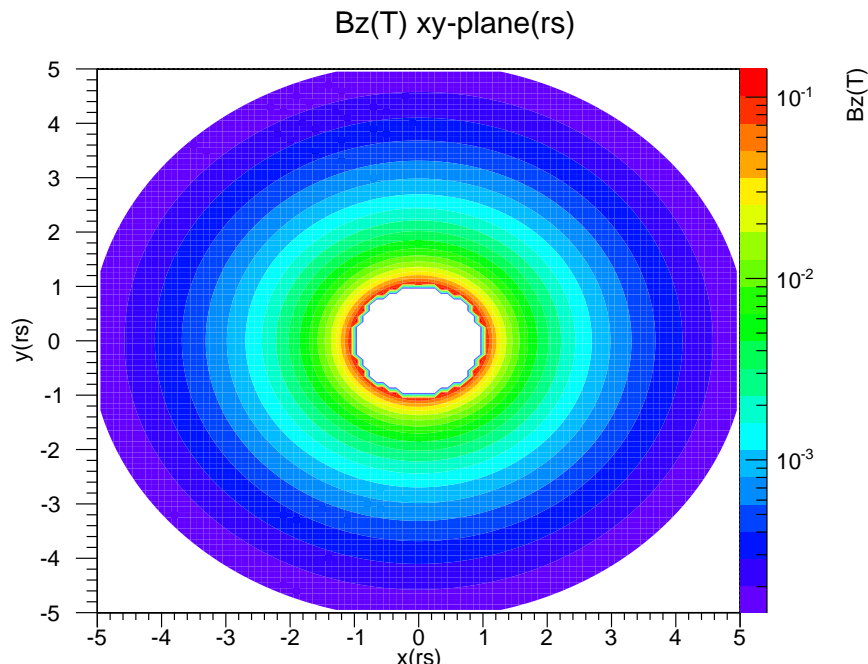


Figure 14: B_z (T) in the xy -plane around the sun.

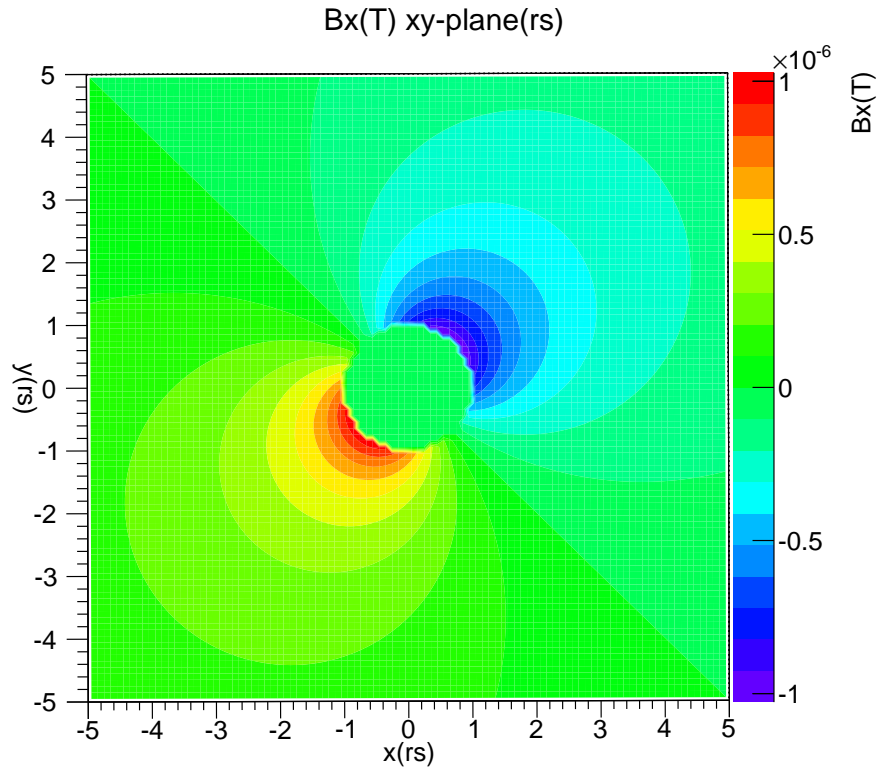


Figure 15: B_x (T) in the xy -plane around the sun.

3.5 RAY TRACING

Due to the deflection of the nuclei by the magnetic field it would take a lot of CPU-time if the simulation just shot particles randomly toward the Earth and calculates if they hit. A less time consuming solution would be to shoot a particle away from the Earth and look where they end up on the 4 AU sphere around the sun. From that point the momentum of the particle can be inverted and the interaction probability of the particle along its path back can be calculated. The ray tracing program is similar to the normal program except for two important changes:

1. The particle starts at Earth and has a momentum directed outward.
2. The charge of the particle is, temporarily, inverted. This is to implement the correct deflection of the nuclei in the magnetic field of the sun.

[Figure 16](#) is an artist impression of the idea of tracing the particles.

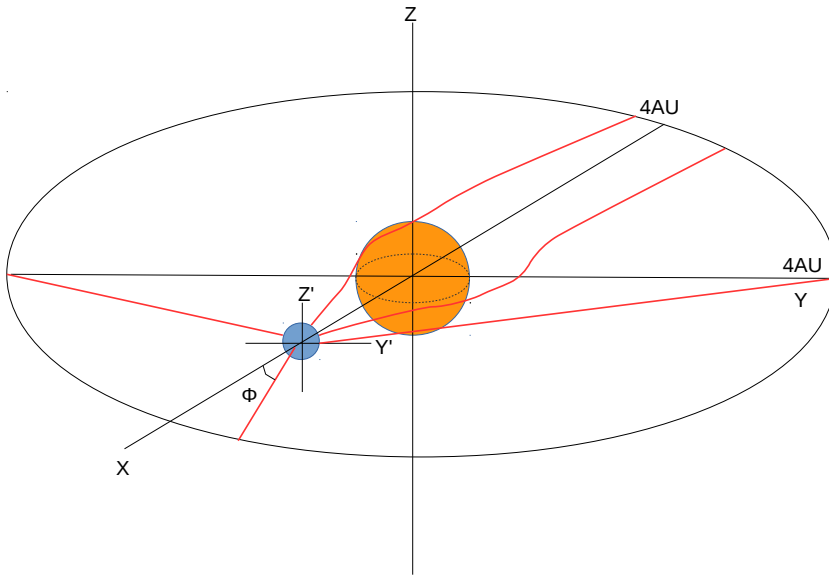


Figure 16: Impression of ray tracing. Particles start with inverted charge at the Earth and are tracked through the magnetic field of the sun to the 4 AU sphere around the sun.

3.6 RESULTS SO FAR

With the knowledge of the previous chapter again a interaction probability can be calculated. But now the program starts with a ray tracing and then uses that path to calculate the total interaction probability along a track towards the Earth. This is done for each nucleus in bins of one degree in each spherical angle starting at the position of the Earth. [Figure 17](#) and [Figure 18](#) show the results of these calculations for iron nuclei with an energy of respectively 0.6 EeV and 0.1 EeV. If you compare these to [Figure 10](#) and [Figure 11](#) of [Chapter 2](#) there are no differences visible. The differences in path traveled by the nuclei hardly influence the total interaction probability.

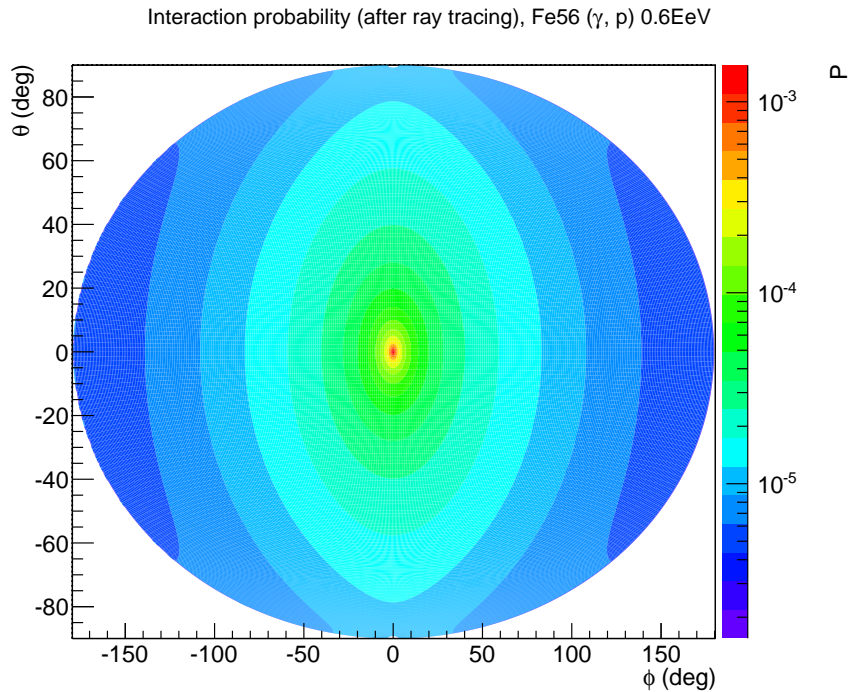


Figure 17: Interaction probability for iron nuclei of 0.6 EeV traveling from a 4 AU sphere around the sun to the Earth. The paths through the sun's magnetic field are found using the ray tracing algorithm described in the text.

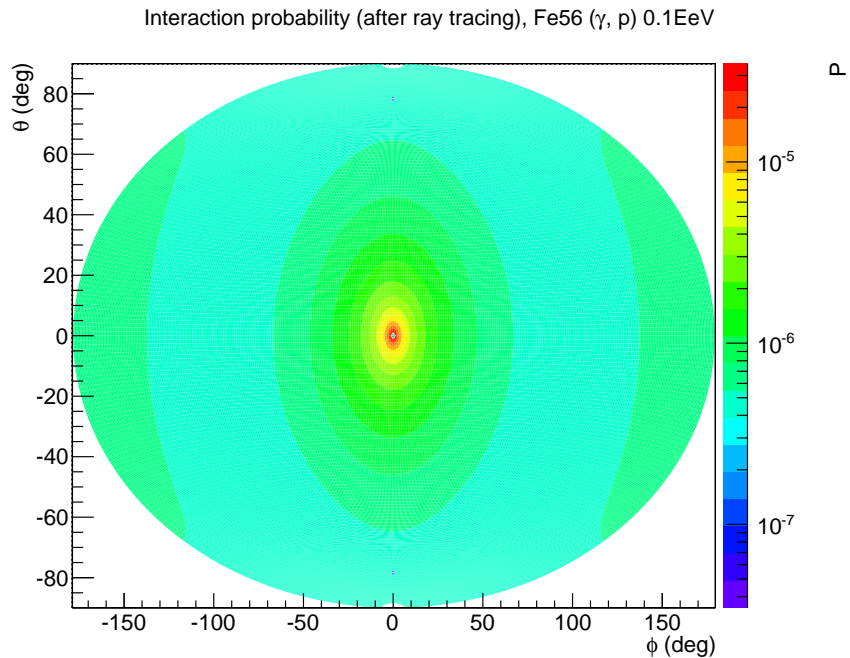


Figure 18: Interaction probability for iron nuclei of 0.1 EeV traveling from a 4 AU sphere around the sun to the Earth. The paths through the sun's magnetic field are found using the ray tracing algorithm described in the text.

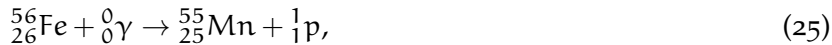
4

INTERACTIONS

Possible G.Z. events can only be properly detected if both secondary particles hit the Earth. Due to the deflection by the interstellar magnetic field this might not be the case. The program is therefore extended by implementing an interaction and tracking of secondary particles.

4.1 FORCED INTERACTIONS

To make sure that an interaction does occur along the path of the nucleus a random number between zero and the maximum interaction probability of that specific track is generated. Therefore, position, momentum and interaction probability are stored in a data file for each point on each track. Next, a search loop in the program finds the point where the interaction probability crosses the random number. At this point an interaction is implemented. This thesis focuses on two interactions



For both interactions the secondary particles are stable.

The following assumptions are made:

1. The energy and momentum of the photon are neglected in the reaction kinematics.
2. The two particles at the point of generation are assumed to travel on parallel paths.
3. The momentum of the initial nucleus is divided over the secondaries proportionally to the fraction of the masses.

The program then tracks the heaviest secondary and checks if it hits the Earth. If it does, it also tracks the lighter particle. This is just to save CPU-time. [Figure 19](#) is an impression of this process. If both secondaries hit the Earth the separation distance on the Earth's surface can be calculated. The interaction probability for the cosmic ray and subsequent detection of its secondaries then becomes a total probability for observing this process.

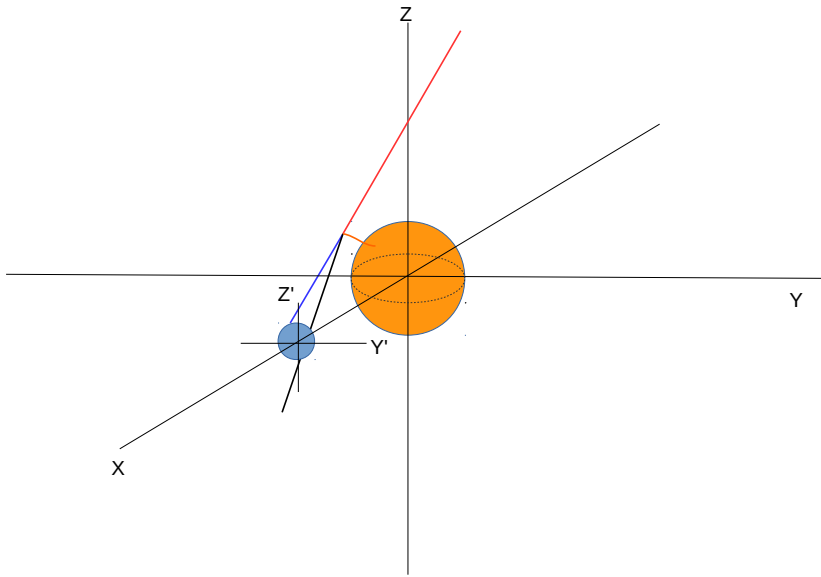


Figure 19: Artist's impression of a primary cosmic ray (in red from the top right) interacting with a photon from the sun, thereby generating secondaries (in blue and black from the interaction point) that might hit the Earth at a certain distance.

4.2 RESULTS SO FAR

For each track 100 interactions as described in [Section 4.1](#) are generated randomly along the path from the 4 AU sphere around the sun to the Earth. The measurement probability is, in this case, the total interaction probability between the point on the 4 AU sphere and the Earth for that track divided by 100. If more particles hit the same spot their measurement probabilities are added. Four plots are presented:

1. [Figure 20](#) The measurement probability of the G.Z. effect for a 0.6 EeV iron nucleus is plotted as a function of the arrival direction of the heaviest secondary.
2. [Figure 21](#) The average distance between the secondaries, created in the G.Z. process for 0.6 EeV iron, is plotted as a function of the arrival direction of the heaviest secondary.
3. [Figure 22](#) The separation distributions for the particles that originate from $(\phi, \theta) = (122, -2)$ on the 4 AU sphere i.e. the tracks are far away from the sun.
4. [Figure 23](#) The separation distributions for the particles that originate from $(\phi, \theta) = (-2, 18)$ on the 4 AU sphere i.e. the tracks that pass close to the sun.

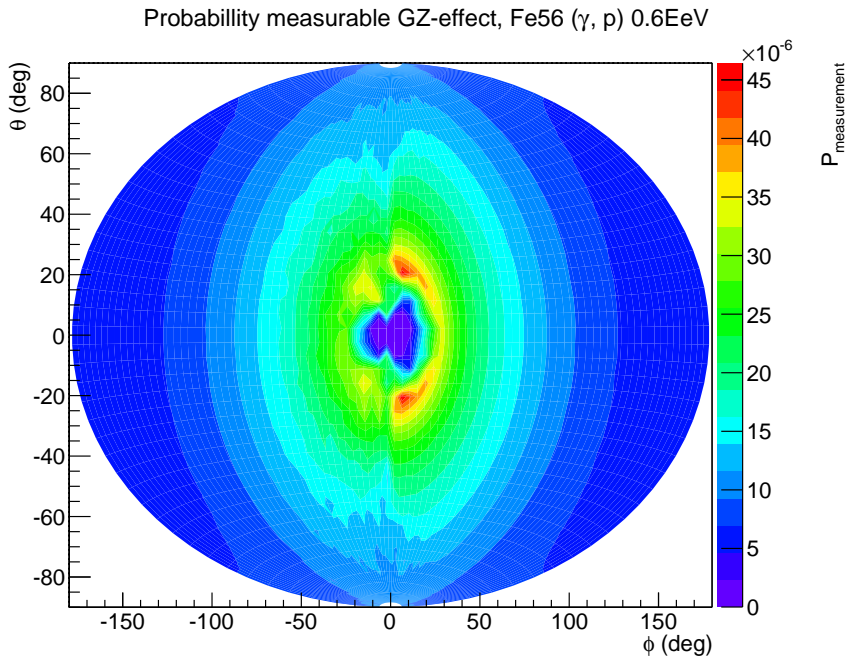


Figure 20: Probability of observing a G.Z. event from a interaction of an iron nucleus of 0.6 EeV on Earth as a function of the arrival direction of the heaviest secondary.

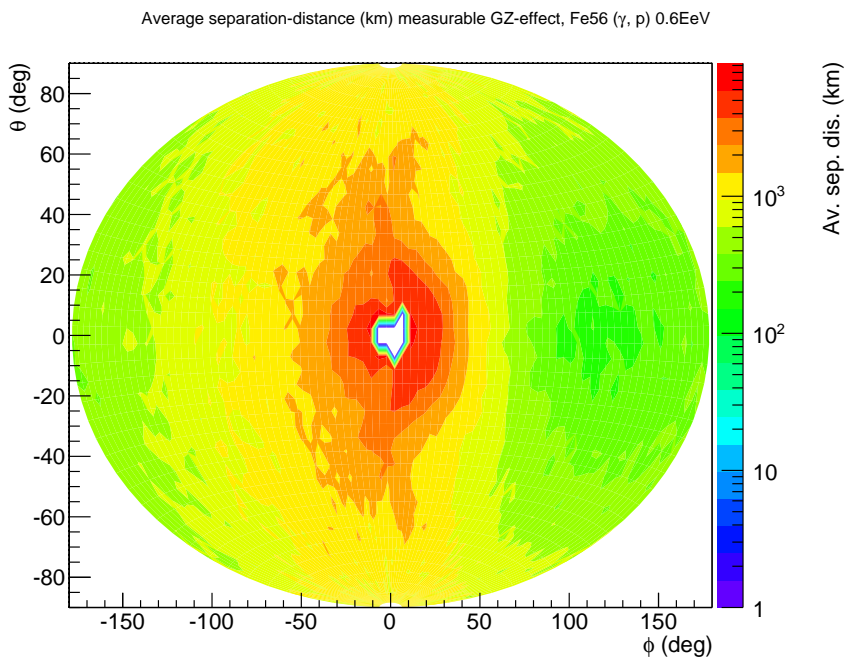


Figure 21: Average separation distance in km of the secondaries from a G.Z. interaction of an iron nucleus of 0.6 EeV on Earth as a function of the arrival direction of the heaviest secondary.

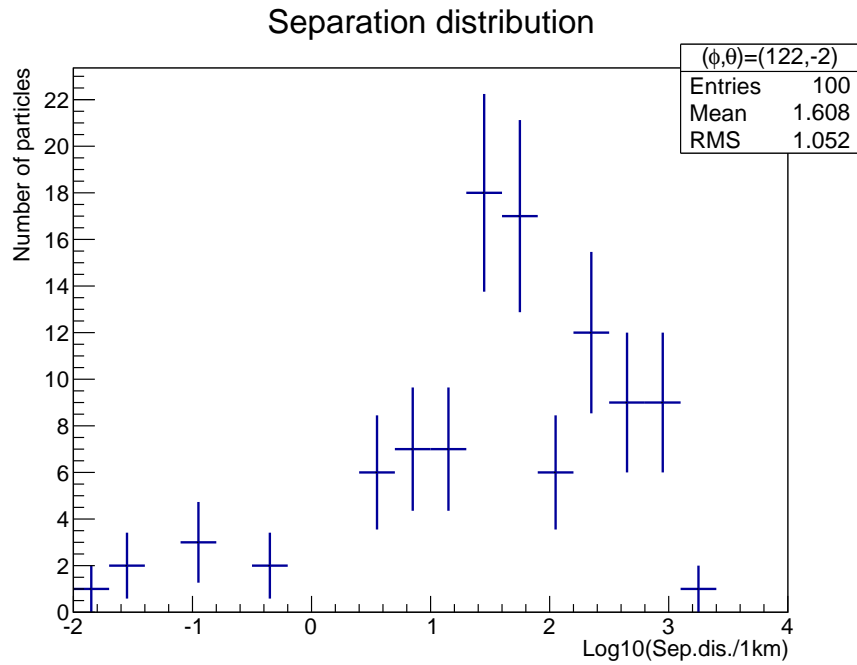


Figure 22: Distribution of the distance between the arrival position of the proton and Mn-55 nucleus on Earth for interactions of 0.6 EeV iron far away from the sun.

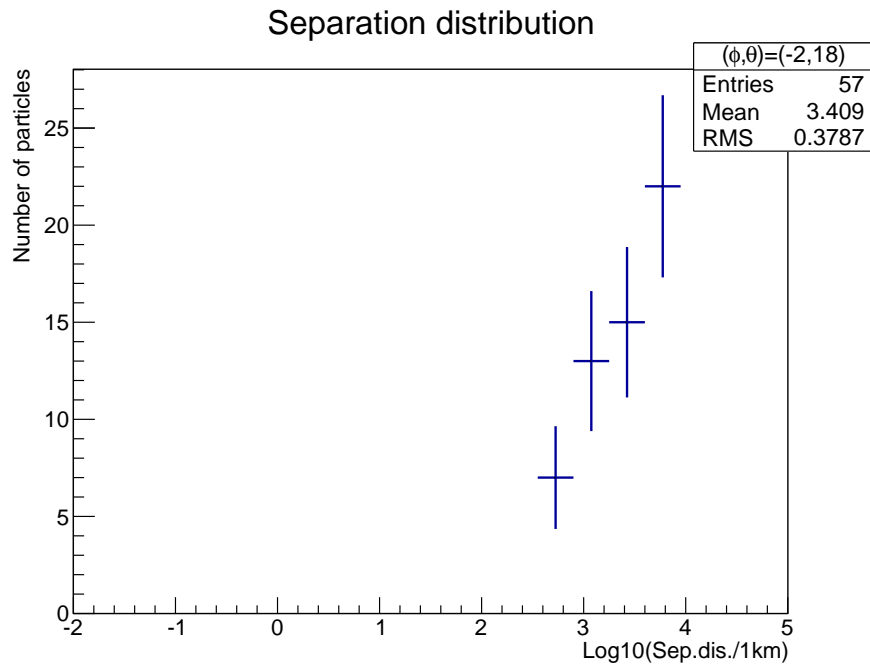


Figure 23: Distributions of the distance between the arrival position of the proton and Mn-55 nucleus on Earth for interactions of 0.6 EeV iron close to the sun.

The probability of observing the heaviest secondary from a G.Z. interaction on Earth is highest for events that come from a direction near the sun. But the separation distance between the fragments on Earth from events near the sun is of the order of 10^3 km. With current detector setups such as HiSPARC, Auger and LAAS it is unlikely that G.Z. events originating near the sun can be measured. Measuring separation distances of the order of 10^2 km is possible. Therefore G.Z. events are more likely to be found in the data collected in a direction away from the sun. This corresponds to the green areas in [Figure 21](#). This will mostly be the data collected during the night time. Excluding the other data will improve the signal over background ratio.

5

G.Z. FLUX RATE ON EARTH

Up until this chapter only considered a nucleus that enters our solar system with a specific direction and energy has been considered. The probability that a particle enters with exactly that direction and energy is extremely small, if not zero. The program is therefore extended with two parts. The first part generates particles with small random variations in direction. The second implements the flux of cosmic rays as a function of energy for the generated phase space.

5.1 SLIGHT VARIATION IN INITIAL DIRECTION

Ray tracing was used to find the direction of the incoming nucleus so that it would hit the Earth. It might be possible that a particle with a slightly different direction may also hit the Earth. A random number generator is used to generate 99 particles with directions close to the original direction. These particles are traced through the solar system in order to figure out if they hit the Earth. To save cpu-time this tracing is first done without implementing interactions along its track. Of course there is a possibility that the secondary particles hit the Earth even if the main nucleus doesn't. To make sure these possibilities are taken into account, the radius of the Earth is overestimated by 20% in this initial tracking. The data of the nuclei that hit this enlarged Earth are used to implement an interaction. From these interactions the secondaries are tracked to check if they actually hit the true Earth. In total 100 particles and 30 interactions per track are generated. Therefore there is a maximum of 3000 G.Z. events per direction that may hit the Earth. The maximum openings angle is chosen so that approximately 1500 G.Z. events from the 'midnight' direction hit the Earth. This is achieved by setting the maximum angular deviation to $1.30208 \cdot 10^{-3}$ degrees.

5.2 COSMIC RAY FLUX

So far, all calculations were performed for several fixed nucleus energies. The next step is to integrate over the energy spectrum of the incoming cosmic ray. This differential energy spectrum of cosmic rays is described by [17]

$$J = C \cdot \left(\frac{E}{6.3 \cdot 10^{18}} \right)^{-3.20 \pm 0.05}, \quad (27)$$

for $4 \cdot 10^{17} \text{ eV} < E < 6.3 \cdot 10^{18} \text{ eV}$,

with

J Differential energy flux of cosmic rays in $\text{km}^{-2} \text{s}^{-1} \text{sr}^{-1} \text{eV}^{-1}$,

$C = (9.23 \pm 0.65) \cdot 10^{-27} \text{ km}^{-2} \text{s}^{-1} \text{sr}^{-1} \text{eV}^{-1}$, and

E The energy of the cosmic ray nucleus in eV.

A plot of this function is found in [Figure 24](#).

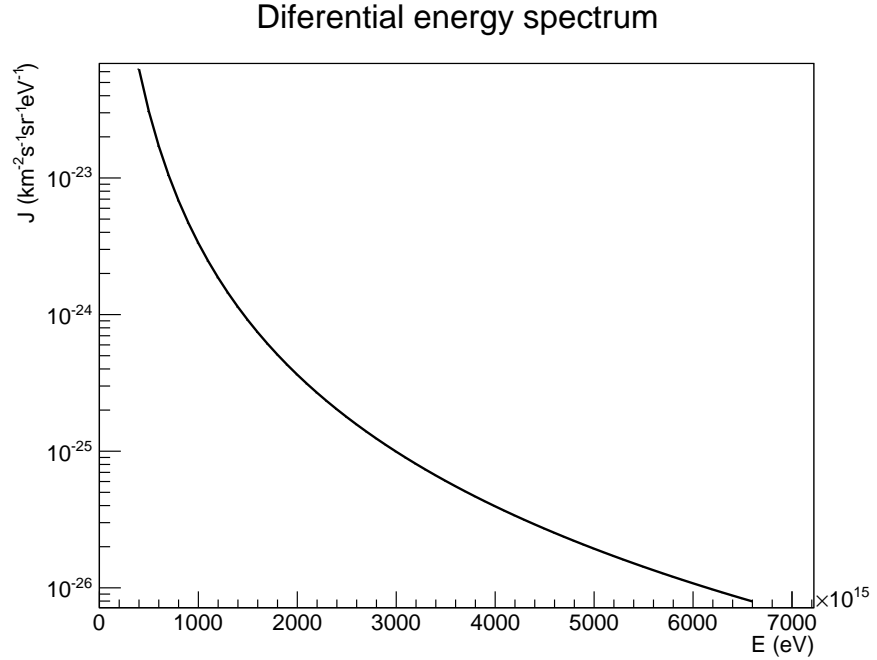


Figure 24: Cosmic ray flux as a function of energy according to [Equation 27](#)

In order to calculate the total flux of cosmic rays between two energy boundaries this differential energy spectrum needs to be integrated

$$\begin{aligned} F &= C \cdot \int_{E_1}^{E_2} \left(\frac{E}{6.3 \cdot 10^{18}} \right)^{-3.20 \pm 0.05} dE \\ &= \frac{C \cdot (6.3 \cdot 10^{18})^{3.20 \pm 0.05}}{(-2.20 \pm 0.03)} \left(E_2^{-2.20 \pm 0.03} - E_1^{-2.20 \pm 0.03} \right). \end{aligned} \quad (28)$$

5.3 G.Z. FLUX RATE

The number of G.Z. events that arrive on Earth per unit time is calculated as follows

$$\text{Rate} = J \sum_i \frac{\#\text{hit}_i}{\#\text{gene.}} P_i \int_{\phi_1=0}^{2\pi} \int_{\theta_1=0}^A R^2 d\phi_1 d(\cos\theta_1) \times \\ \int_{\phi_2=0}^{2\pi} \int_{\theta_2=0}^B d\phi_2 d(\cos\theta_2), \quad (29)$$

with

- i the sum is made for all pairs produced for one area on the 4 AU sphere around the sun and reaching the Earth, a particle is generated each 15 degrees in a (θ, ϕ) grid,
- J the differential energy flux see [Equation 27](#),
- $\#\text{hit}_i$ the number of G.Z. events that hit the Earth from that track,
- $\#\text{gene.}$ the generated number of G.Z. events in that track. In this case 100 different openings angles with each 30 interactions, a total of 3000 tracks for each sampled point on the 4 AU sphere around the sun,
- P_i the total interaction probability for that specific track,
- R the radius, 4 AU,
- A the maximum openings angle the generated particles could have compared to that specific track ($1.30208 \cdot 10^{-3}$ degrees), and
- B the leading particle is assumed to be typical for particles originating from a surface of $2\pi R^2 (1 - \cos(B))$ with $B = 7.5$ degrees.

When calculating the integrated flux, J from [Equation 27](#) is replaced by F from [Equation 28](#).

5.4 RESULTS SO FAR

Equation 29 is used in the simulation to calculate the rate of G.Z. events that hit the Earth for different primary energies. For each energy around $5.7 \cdot 10^5$ G.Z. secondaries are generated. For iron primaries this procedure is followed for 19 different energies. For oxygen primaries 33 different energies are generated. The data collected occupied around 384 gigabytes. From these data two plots are extracted:

1. Figure 25 shows the differential rate of G.Z. pairs that hit the Earth each second, assuming all primary cosmic rays are Fe-56. Note that the line is plotted to guide the eye through the calculated data points. In total 0.87 G.Z. events hit the Earth each second under these assumptions.
2. Figure 26 shows the differential rate of G.Z. pairs that hit the Earth each second, assuming all primary cosmic rays are O-16. Note that the line is plotted to guide the eye through the calculated data points. In total 1.7 G.Z. events hit the Earth each second under these assumptions.

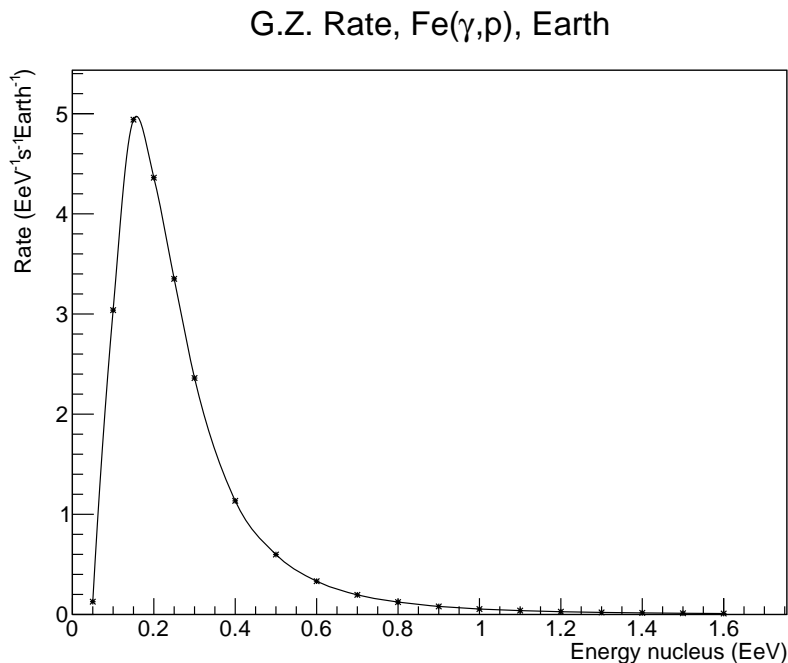


Figure 25: Differential rate of G.Z. events reaching the Earth as a function of energy, assuming that the full flux consists of iron.

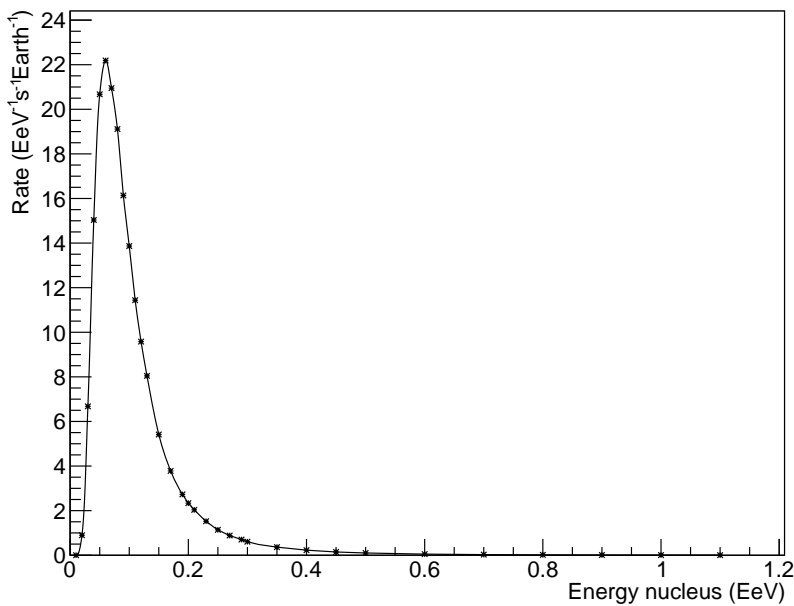
G.Z. Rate, O(γ ,p), Earth

Figure 26: Differential rate of G.Z. events reaching the Earth as a function of energy, assuming that the full flux consists of oxygen.

6

DETECTOR CONFIGURATION

In [Chapter 5](#) the rate of G.Z. events that hit the Earth each second was calculated. Unfortunately not the entire Earth can be used as a detector. Therefore the program is extended again. This time to implement detector setups similar to Auger and HiSPARC.

6.1 PIERRE AUGER

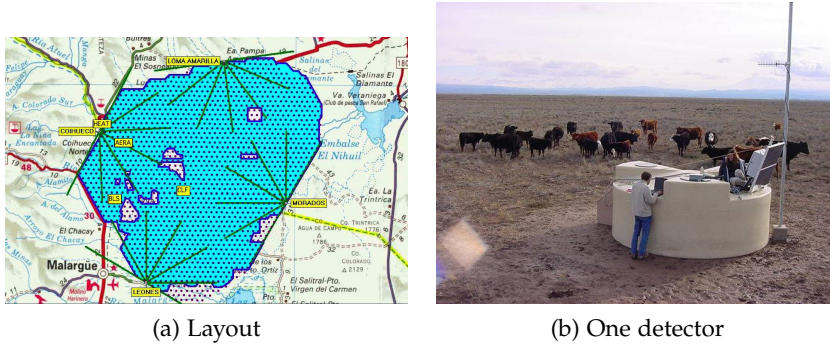


Figure 27: The layout of the Pierre Auger observatory on the Pampa Amarilla (a). Each dot is a water Cherenkov tank particle detector as shown in (b). The green lines from the side are the segment indications for the fluorescence detectors that overlook the array. [\[18\]](#)

The Pierre Auger observatory is situated in Argentina and covers an area of roughly 3000 km^2 (see [Figure 27](#)). Not the complete Auger detector is modeled, instead we investigated a $60 \times 50 \text{ km}$ surface that could be anywhere on Earth. The probability that a nucleus hits this surface is:

$$P = \frac{A_{\text{detector}}}{A_{\text{Earth}}} = \frac{3000}{5.1 \cdot 10^8} = 5.88 \cdot 10^{-6} \quad (30)$$

The probability that the second nucleus also hits this surface depends on the separation distance between the two particles. If the separation distance is larger than the diagonal of the detector area i.e. $\sqrt{50^2 + 60^2} = 78.1 \text{ km}$ the probability of detection is zero. Any closer, the probability depends on the fraction of detector area available for this distance. This distribution is calculated in a different program. The result is shown in [Figure 28](#).

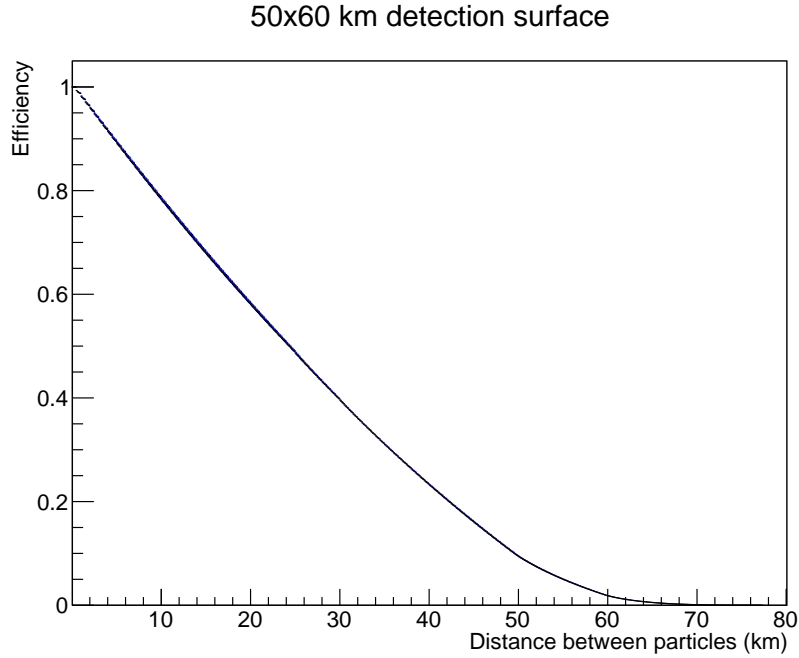


Figure 28: The probability for the second secondary to fall into a 60×50 km area once the first secondary is detected in the same particle area.

6.2 RESULTS SO FAR

The rate, [Section 5.3 Equation 29](#) is multiplied by both the probability for the first and second particle to fall in the detector area.

Again two plots are presented:

1. [Figure 29](#) shows the differential rate of G.Z. pairs that hit a 3000 km^2 detector surface each year, assuming all primary cosmic rays are Fe-56. Note that the line is plotted to guide the eye through the calculated data points. In total 6.5 G.Z. events hit a 3000 km^2 surface each year under these assumptions.
2. [Figure 30](#) shows the differential rate of G.Z. pairs that hit a 3000 km^2 detector surface each year, assuming primary all cosmic rays are O-16. Note that the line is plotted to guide the eye through the calculated data points. In total 14 G.Z. events hit a 3000 km^2 surface each year under these assumptions.

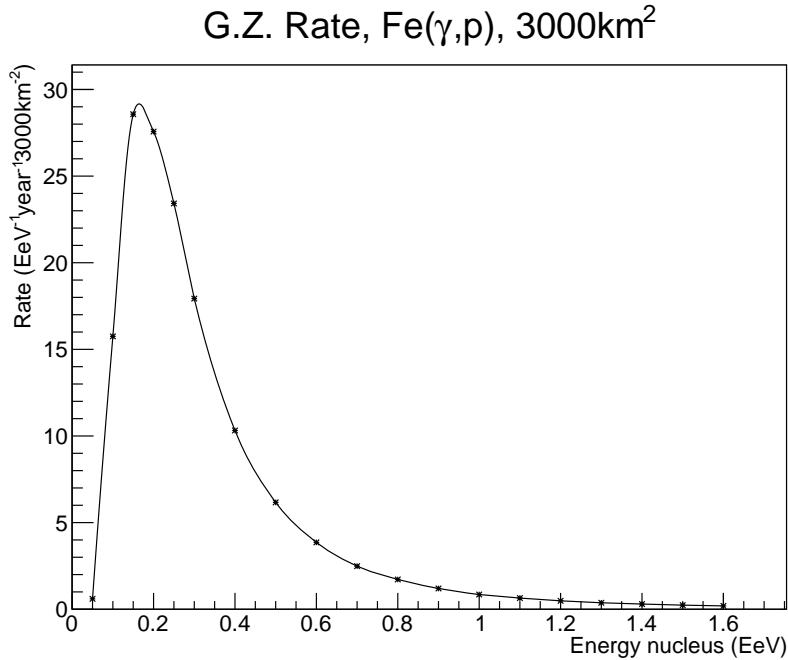


Figure 29: Differential rate of G.Z. events recorded by a 3000 km 2 detector as a function of energy, assuming that the full flux consists of iron.

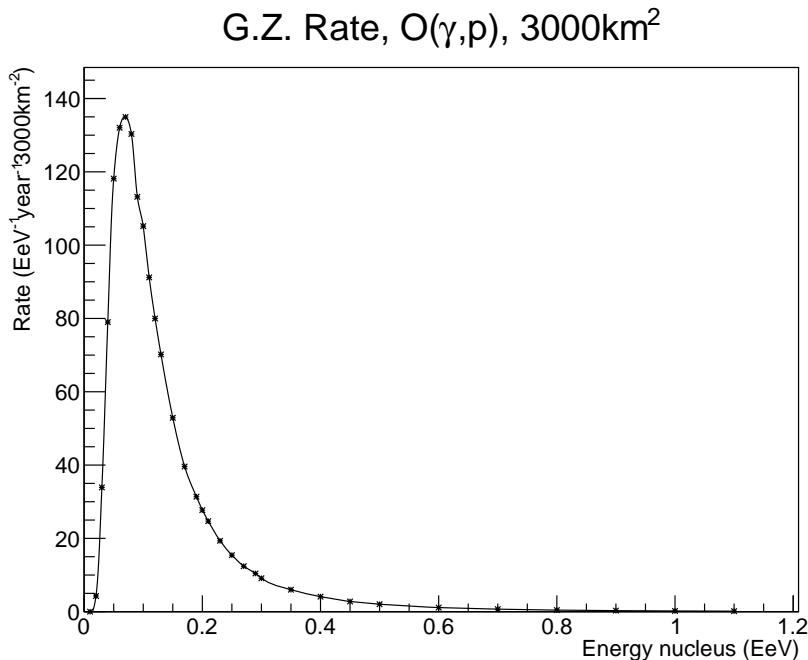


Figure 30: Differential rate of G.Z. events recorded by a 3000 km 2 detector as a function of energy, assuming that the full flux consists of oxygen.

6.3 HISPARC

HiSPARC stands for High School Project on Astrophysics Research with Cosmics. The detector array currently consists of 119 detector stations placed on participating high schools and universities.

We implemented a HiSPARC configuration that could be situated anywhere on the Earth. The probability for the first nucleus to be measured by one station depends on the total observatory surface. This observatory surface is larger than the surface of all the detectors added. There is an area around each detector where a shower can be created that the detector will be sensitive to. This distance depends on the energy of the shower. The correlation is studied by dr. Fokkema [19] and the result is shown in [Figure 32](#).

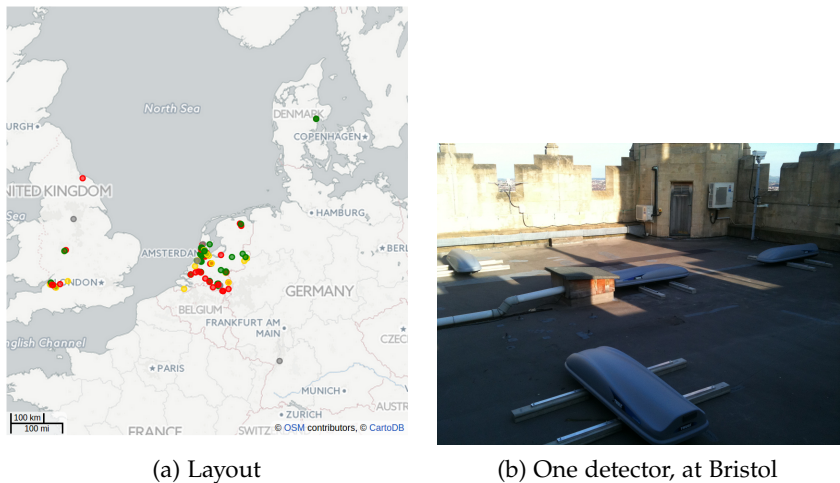


Figure 31: HiSPARC observatory.[[20](#)]

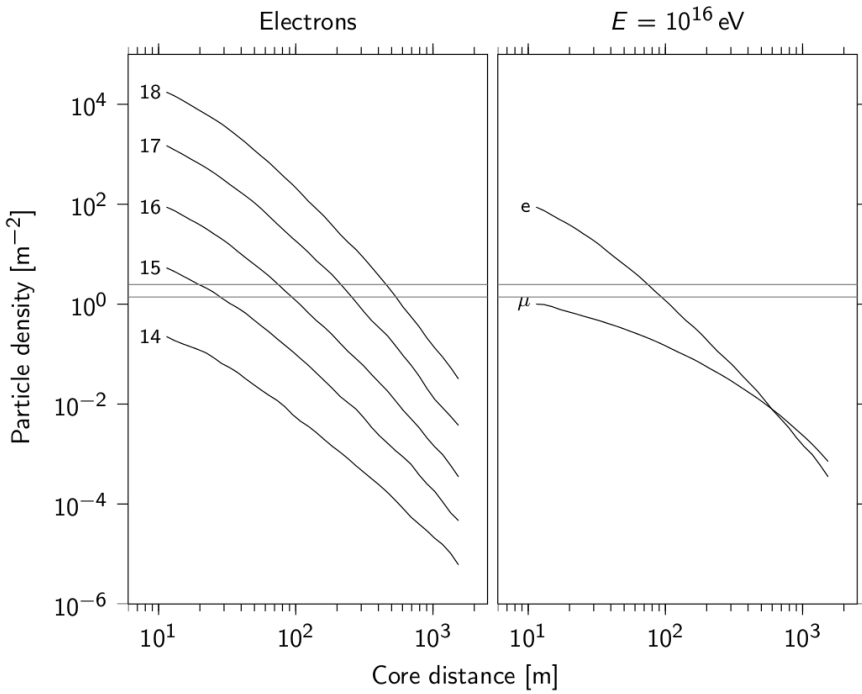


Figure 32: Figure copied from [19]. "Lateral distribution functions (LDFs) for proton-induced EAS. The LDF is summed over electrons and positrons for primary energies ranging from 10^{16} eV to 10^{18} eV (left). The two horizontal lines show the particle densities of 1.39 m^{-2} and 2.46 m^{-2} , i.e. the 50% detection probabilities for one and two detectors, respectively. (...)"

From these results, a detection distance of 0.5 km is taken as a upper limit for a cosmic ray energy of 10^{18} eV.

The probability for the first nucleus to hit a HiSPARC station is then:

$$P = \frac{A_{\text{detector}}}{A_{\text{Earth}}} = \frac{119 \cdot \pi \cdot 0.5^2}{5.1 \cdot 10^8} = 1.8 \cdot 10^{-7} \quad (31)$$

The probability for the second nucleus to hit another station depends on the separation distance between the two nuclei. To calculate this probability the surface distribution of all combinations of stations is calculated. The result is shown in Figure 33.

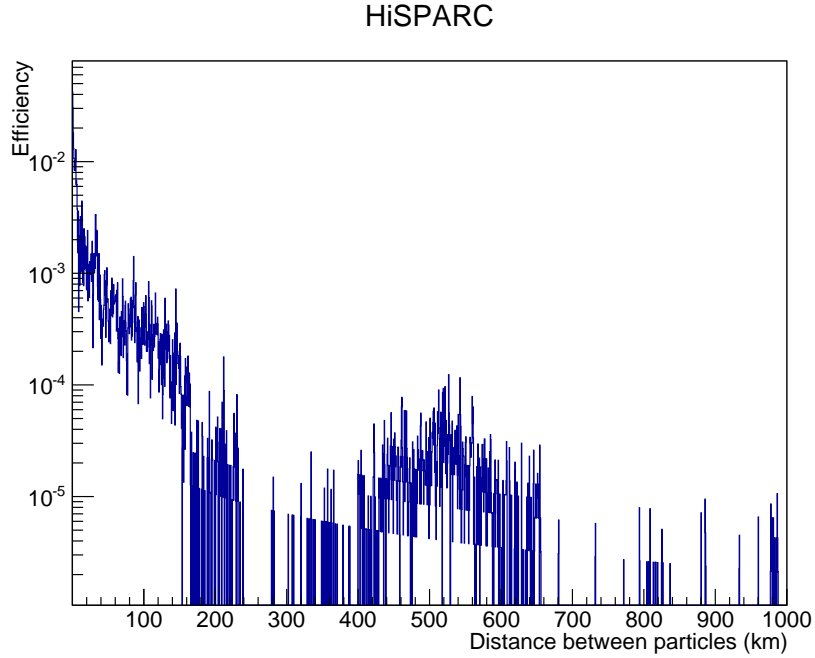


Figure 33: Probability to detect the second nucleus with HiSPARC configuration given that the first secondary has been detected by HiSPARC.

6.4 RESULTS SO FAR

The rate, [Section 5.3 Equation 29](#) is multiplied by both the probability for the first and second particle to fall in the detector area.

Again two plots are presented:

1. [Figure 34](#) shows the differential rate of G.Z. pairs that hit the Hisparc configuration each year, assuming all primary cosmic rays are Fe-56. Note that the line is plotted to guide the eye through the calculated data points. In total 4.9 G.Z. events hit a HiSPARC configuration every 1000 years under these assumptions.
2. [Figure 35](#) shows the differential rate of G.Z. pairs that hit the HiSPARC configuration each year, assuming all primary cosmic rays are O-16. Note that the line is plotted to guide the eye through the calculated data points. In total 10 G.Z. events hit a HiSPARC configuration every 1000 years under these assumptions.

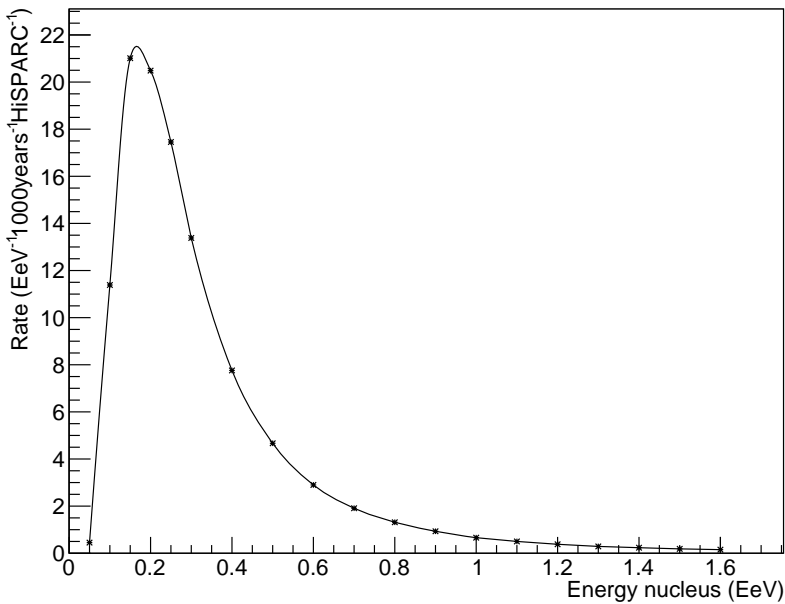
G.Z. Rate, Fe(γ ,p), HiSPARC configuration

Figure 34: Differential rate of G.Z. events for which the two secondaries detected by HiSPARC, assuming that the full flux consists of iron.

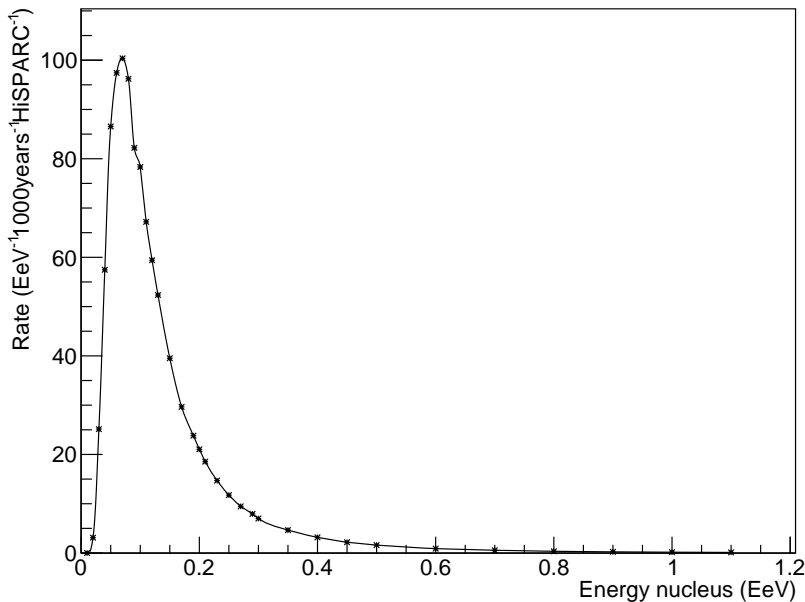
G.Z. Rate, O(γ ,p), HiSPARC configuration

Figure 35: Differential rate of G.Z. events for which the two secondaries detected by HiSPARC, assuming that the full flux consists of oxygen.

7

CONCLUSIONS

7.1 THE GERASIMOVA-ZATSEPIN EFFECT

This thesis concludes that it should be possible to detect the G.Z. effect on Earth. If you measure toward the sun the expected number of events is higher but the average separation distance, due to the interstellar magnetic field, is also much larger. Depending on the detector configuration it might be necessary to exclude data from day or nighttime to improve the signal over background ratio. The highest rate for Fe-56 primaries is found around an energy of the primary nucleus of 0.15 EeV. For O-16 primaries it is around 0.07 EeV. Note that the secondaries have a fraction of this energy. Since an interaction was studied in which a proton is expelled this proton has the lowest energy. In the simulation, the proton originating from primary iron has an energy of $\frac{1}{56} \cdot 0.15 \text{ EeV} = 2.7 \text{ PeV}$. The energy of the proton from a primary oxygen is $\frac{1}{16} \cdot 0.07 \text{ EeV} = 4.4 \text{ PeV}$.

7.2 CURRENT DETECTOR SETUPS

The calculated G.Z. rates that can be detected by an Auger or HiSPARC like setup are upper limits. In reality this rate will be lower. This due to the assumptions that were made in our approach. Therefore it is safe to conclude that with the current detector setups like Auger and HiSPARC it is impossible to measure the G.Z. effect with any statistical significance. However, you might be lucky to record an event. Note that the proton energy is so low that the detection efficiency for HiSPARC is overestimated, see [Section 6.3](#). Furthermore, the Auger detector has an energy threshold beyond 10^{18} eV [21], therefore the G.Z. effect cannot be measured by Auger.

7.3 COMPARED WITH EARLIER RESULTS

As mentioned in the introduction a number of theoretical studies have been performed [2, 3, 4, 5, 6, 7]. The calculated G.Z. rates in this thesis are in rough agreement with the results of these studies. These studies also conclude that the probability of observing the heaviest secondary from a G.Z. interaction is the highest for events that come from a direction away from the sun i.e. the night side. This might be due to the deflection of the particles in the magnetic field and therefore missing the Earth. By the use of ray tracing as explained in

[Section 3.5](#) this thesis concludes that the probability of observing the heaviest secondary from a G.Z. interaction on Earth is the highest for events that come from a direction near the sun. But the separation distance between the fragments on Earth from events originated near the sun is of the order of 10^3 km. The question arises what the best detector setup might be. The last section of this thesis focuses on answering this question.

7.4 WHAT IF ...

What if there was the possibility to design a detector than can measure the G.Z. effect. Of course there are no unlimited resources so it has to be as cheap as possible. What would be the design?

The previous sections show that the detector should have an energy threshold of about one PeV. However this requires one PeV showers to be measured properly, and therefore detector stations placed at short distance to each other.

It is also useful to look at the separation distribution rate of the generated data. [Figure 36](#) is a plot for Fe-56 and [Figure 37](#) for O-16.

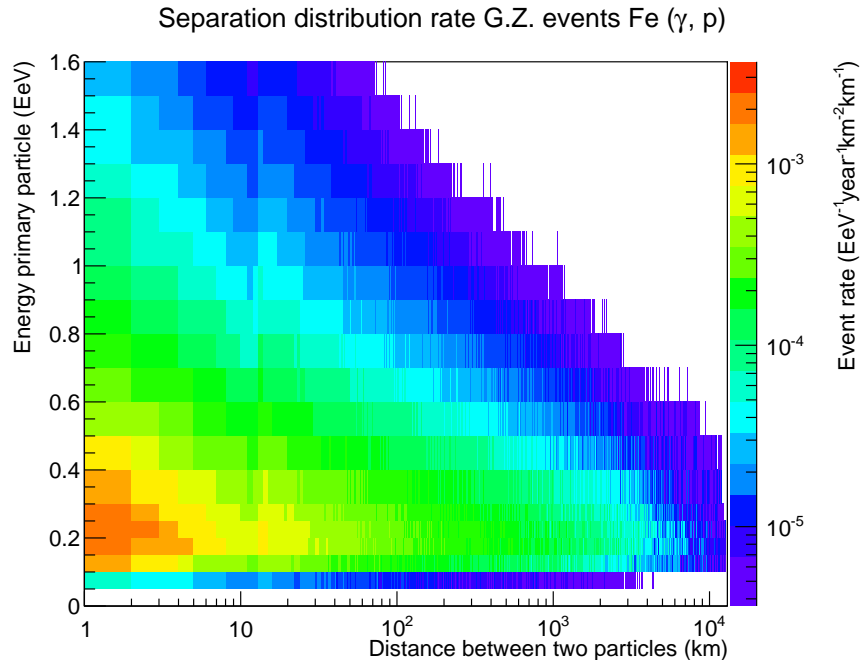


Figure 36: Differential event rate as function of energy and separation distance if the flux entirely consists of Fe-56 nuclei.

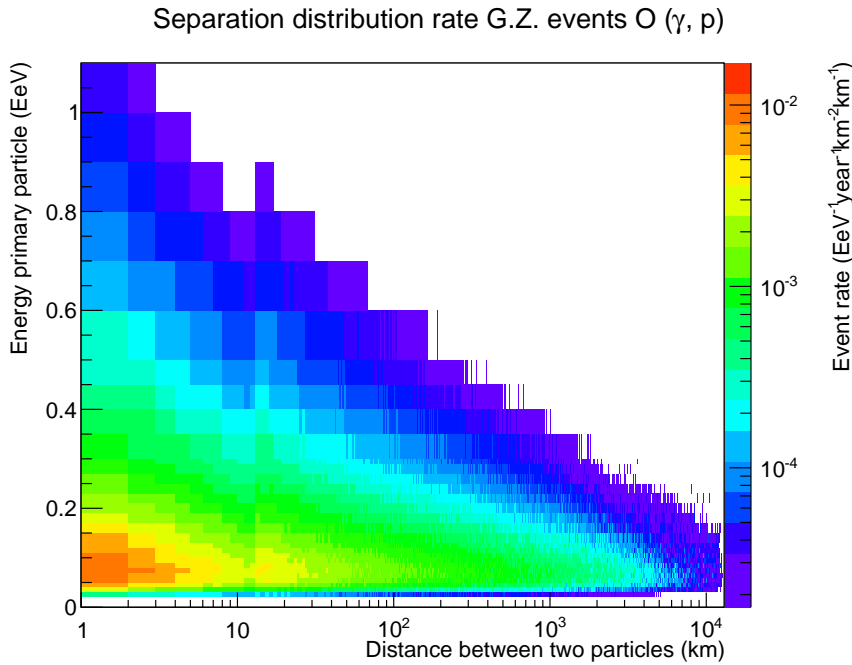


Figure 37: Differential event rate as function of energy and separation distance if the flux entirely consists of O-16 nuclei.

For oxygen primaries shown in Figure 37 a slight increase in the rate is visible around a separation distance of 20 km. This is also present for iron primaries. The origin of this effect is not known. The arrival direction distributions of these events do not indicate any special features.

Figure 36 and Figure 37 show that the detector has to be sensitive to particle distances of about one kilometer. The footprint size with a detection threshold of 0.1 particle per square meter is approximately 200 m, hence two separate showers with a 1 km separation should be well distinguishable. Proper detection requires more than 5 measurements well within the 200 m radius footprint of the showers, hence a detector station density of 40 stations per square kilometer or about 160 m between stations. In that case the total surface has to be covered to measure 10 events per year is about 5000 km^2 for oxygen primaries. Let's assume this detector is a square, the maximum separation distance of the secondaries for a possible detection is 100 km. To improve the signal over background the G.Z. rate of primary oxygen as a function of the arrival direction of the heaviest secondary, if the separation between the two secondaries on Earth is less than 100 km, is plotted in Figure 38. This was achieved by integrating the differential energy flux of cosmic rays as explained in Section 5.2. The result shows that for these separation distances between secondaries of G.Z. events the preferred direction for observing is away from the sun. For an upward looking observatory, this means observing at night.

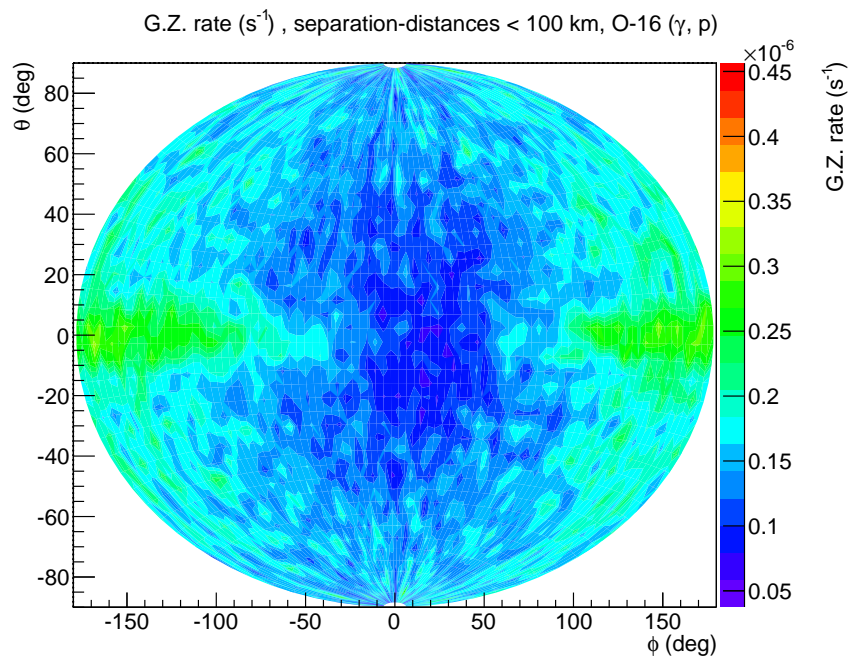


Figure 38: The integrated G.Z. rate of primary oxygen as a function of the arrival direction of the heaviest secondary if the separation between the two secondaries on Earth is less than 100 km.

A

APPENDIX A

Stefan-Boltzmann's law from Planck's law.

To calculate the effective temperature of the photosphere of the sun we use Stefan-Boltzmann's law. In this appendix Stefan-Boltzmann's law is derived starting from Planck's law for the energy flux density

$$d\Phi(\nu, T) = \frac{2\pi h\nu^3}{c^2} \frac{1}{e^{h\nu/k_B T} - 1} d\nu.$$

We first integrate this for the number of photons above a frequency ν_0 ,

$$\begin{aligned} \Phi(\nu > \nu_0) &= \int_{\nu_0}^{\infty} \frac{d\Phi(\nu)}{d\nu} d\nu \\ &= \int_{\nu_0}^{\infty} \frac{2\pi h\nu^3}{c^2} \frac{1}{e^{h\nu/kT} - 1} d\nu \\ &= \frac{2\pi h}{c^2} \int_{\nu_0}^{\infty} \frac{\nu^3}{e^{h\nu/kT} - 1} d\nu \\ &= \frac{2\pi h(kT)^4}{h^4 c^2} \int_{h\nu_0/kT}^{\infty} \frac{(h\nu/kT)^3}{e^{h\nu/kT} - 1} d(h\nu/kT). \end{aligned}$$

To solve this we use

$$\begin{aligned}
\int_a^{\infty} \frac{x^3 e^{-x}}{1 - e^{-x}} dx &= \int_a^{\infty} x^3 \sum_{n=1}^{\infty} e^{-nx} dx. \\
&= \sum_{n=1}^{\infty} \int_a^{\infty} x^3 e^{-nx} dx \\
&= \sum_{n=1}^{\infty} \frac{-1}{n} \int_a^{\infty} x^3 d e^{-nx} \\
&= \sum_{n=1}^{\infty} \left[\frac{-1}{n} x^3 e^{-nx} \Big|_{x=a}^{\infty} + \frac{1}{n} \int_a^{\infty} e^{-nx} d x^3 \right] \\
&= \sum_{n=1}^{\infty} \left[\frac{a^3 e^{-na}}{n} - \frac{3}{n^2} \int_a^{\infty} x^2 d e^{-nx} \right] \\
&= \sum_{n=1}^{\infty} \left[\frac{a^3 e^{-na}}{n} - \frac{3}{n^2} \left(x^2 e^{-nx} \Big|_{x=a}^{\infty} - \int_a^{\infty} e^{-nx} d x^2 \right) \right] \\
&= \sum_{n=1}^{\infty} \left[\frac{a^3 e^{-na}}{n} - \frac{3a^2 e^{-na}}{n^2} - \frac{6}{n^3} \int_a^{\infty} x d e^{-nx} \right] \\
&= \sum_{n=1}^{\infty} \left[\frac{a^3 e^{-na}}{n} - \frac{3a^2 e^{-na}}{n^2} - \frac{6}{n^3} \left(x e^{-nx} \Big|_{x=a}^{\infty} - \int_a^{\infty} e^{-nx} d x \right) \right] \\
&= \sum_{n=1}^{\infty} \left[\frac{a^3 e^{-na}}{n} - \frac{3a^2 e^{-na}}{n^2} + \frac{6ae^{-na}}{n^3} + \frac{6e^{-na}}{n^4} \right] \\
&= -a^3 \ln(e^{-a} (e^a - 1)) - 3a^2 \text{Li}_2(e^{-a}) + 6a \text{Li}_3(e^{-a}) + 6 \text{Li}_4(e^{-a}),
\end{aligned}$$

where in turn we have used [22]

$$\frac{e^{-x}}{1 - e^{-x}} = \sum_{n=1}^{\infty} e^{-nx},$$

and the polylogarithms

$$\text{Li}_n(z) = \sum_{k=1}^{\infty} \frac{z^k}{k^n},$$

to proceed

$$\begin{aligned}
\Phi(\nu > \nu_0) &= \frac{2\pi h(kT)^4}{h^4 c^2} \int_{h\nu_0/kT}^{\infty} \frac{(h\nu/kT)^3}{e^{h\nu/kT} - 1} d(h\nu/kT) \\
&= \frac{2\pi h(kT)^4}{h^4 c^2} \sum_{n=1}^{\infty} \left[\frac{(h\nu_0/kT)^3 e^{-n(h\nu_0/kT)}}{n} - \frac{3(h\nu_0/kT)^2 e^{-n(h\nu_0/kT)}}{n^2} \right. \\
&\quad \left. + \frac{6(h\nu_0/kT)e^{-n(h\nu_0/kT)}}{n^3} + \frac{6e^{-n(h\nu_0/kT)}}{n^4} \right] \\
&= \frac{2\pi h(kT)^4}{h^4 c^2} \left[-\left(\frac{h\nu_0}{kT} \right)^3 \ln \left(1 - e^{-(h\nu_0/kT)} \right) - 3 \left(\frac{h\nu_0}{kT} \right)^2 \text{Li}_2(e^{-h\nu_0/kT}) \right. \\
&\quad \left. + 6 \frac{h\nu_0}{kT} \text{Li}_3(e^{-h\nu_0/kT}) + 6 \text{Li}_4(e^{-h\nu_0/kT}) \right].
\end{aligned}$$

The total energy flux from the surface of the sun is then given by

$$\Phi(\nu > 0) = \frac{2\pi h(kT)^4}{h^4 c^2} 6 \text{Li}_4(e^0) = \frac{2\pi^5 k^4 T^4}{15 h^3 c^2}.$$

The effective temperature is

$$T = \sqrt[4]{\frac{\Phi}{\sigma}},$$

with

Φ total power radiated at all frequencies per square meter from a blackbody

radiator, and

σ Stefan-Boltzmann's constant $\frac{2\pi^5 k^4}{15 h^3 c^2} = 5.67 \cdot 10^{-8} \text{ Js}^{-1} \text{ m}^{-2} \text{ K}^{-4}$.

B

APPENDIX B

Transformation of photon energy from rest frame of the sun to the rest frame of the incident nucleus.

The photon energy in the solar rest frame, ϵ , is transformed to the rest frame of the nucleus ϵ^* . E_{ph} , and \vec{P}_{ph} , and E_N , and \vec{P}_N are the energy and momentum of respectively the photon and the nucleus in the rest frame of the sun. The same quantities in the rest frame of the nucleus are marked with a star, *, superscript.

The invariant mass squared calculated in the rest frame of the sun is

$$\begin{aligned} S &= (E_{ph} + E_N)^2 - (\vec{P}_{ph} \cdot c + \vec{P}_N \cdot c)^2, \\ &= (E_{ph} + E_N)^2 - (P_{ph}^2 c^2 + P_N^2 c^2 + 2P_{ph} P_N c^2 \cos \alpha), \\ &= E_{ph}^2 + E_N^2 + 2E_{ph} E_N - P_{ph}^2 c^2 - P_N^2 c^2 - 2P_{ph} P_N c^2 \cos \alpha, \end{aligned}$$

where α is the angle between the photon and the nucleus momenta in the rest frame of the sun.

Using $E^2 = P^2 c^2 + m^2 c^4$ and $m_{ph} = 0$ the expression becomes

$$\begin{aligned} S &= P_{ph}^2 c^2 + P_N^2 c^2 + m_N^2 c^4 + 2\sqrt{P_{ph}^2 c^2} \sqrt{P_N^2 c^2 + m_N^2 c^4} - P_{ph}^2 c^2 \\ &\quad - P_N^2 c^2 - 2P_{ph} P_N c^2 \cos \alpha, \\ &= m_N^2 c^4 + 2P_{ph} c \sqrt{P_N^2 c^2 + m_N^2 c^4} - 2P_{ph} P_N c^2 \cos \alpha. \end{aligned}$$

The same invariant mass squared calculated in the rest frame of the nucleus is

$$\begin{aligned} S &= (E_{ph}^* + E_N^*)^2 - (P_{ph}^* \cdot c)^2, \\ &= E_{ph}^{*2} + E_N^{*2} + 2E_{ph}^* E_N^* - P_{ph}^{*2} c^2, \\ &= P_{ph}^{*2} c^2 + m_N^2 c^4 + 2\sqrt{P_{ph}^{*2} c^2} \sqrt{m_N^2 c^4} - P_{ph}^{*2} c^2, \\ &= m_N^2 c^4 + 2P_{ph}^* m_N c^3, \end{aligned}$$

so

$$P_{ph}^* = \frac{S - m_N^2 c^4}{2m_N c^3}.$$

Fill in the invariant mass squared found in the rest frame of the sun

$$\begin{aligned} P_{ph}^* &= \frac{m_N^2 c^4 + 2P_{ph}c\sqrt{P_N^2 c^2 + m_N^2 c^4} - 2P_{ph}P_N c^2 \cos \alpha - m_N^2 c^4}{2m_N c^3}, \\ &= \frac{P_{ph}\sqrt{P_N^2 + m_N^2 c^2} - P_{ph}P_N \cos \alpha}{m_N c}. \end{aligned}$$

In natural units, with $c = 1$ and $\hbar = 1$, this gives

$$P_{ph}^* = \frac{P_{ph}\sqrt{P_N^2 + m_N^2} - P_{ph}P_N \cos \alpha}{m_N}.$$

And in these natural units, $\epsilon^* = E_{ph}^* = P_{ph}^*$,

$$\epsilon^* = \frac{\epsilon\sqrt{P_N^2 + m_N^2} - \epsilon P_N \cos \alpha}{m_N}.$$

C

APPENDIX C

The effect of a magnetic field on the momentum of a relativistic particle.

Due to the magnetic fields of the sun the direction of momentum of the traveling particle changes along its path. A relativistic momentum change is calculated with

$$dP^\mu = qF^{\mu\nu}U_\nu d\tau,$$

where

dP^μ change in four momentum,

q charge of the particle,

$F^{\mu\nu}$ electromagnetic field tensor, in contravariant matrix form,

$$\begin{bmatrix} 0 & -E_x/c & -E_y/c & -E_z/c \\ E_x/c & 0 & -B_z & B_y \\ E_y/c & B_z & 0 & -B_x \\ E_z/c & -B_y & B_x & 0 \end{bmatrix}$$

U_ν covariant relativistic four-velocity,

$(\gamma, -\gamma v_1, -\gamma v_2, -\gamma v_3)$, and

$d\tau$ proper time interval (dt/γ) .

Note that only magnetic fields are taken into consideration, resulting in

$$dP^\mu = q \begin{bmatrix} 0 & 0 & 0 & 0 \\ 0 & 0 & -B_z & B_y \\ 0 & B_z & 0 & -B_x \\ 0 & -B_y & B_x & 0 \end{bmatrix} (\gamma, -\gamma v_1, -\gamma v_2, -\gamma v_3) d\tau.$$

Multiplying the tensor and the relativistic four-velocity results in

$$d\vec{P} = q\gamma (\vec{v} \times \vec{B}) d\tau.$$

In the reference system of the sun

$$d\vec{P} = q (\vec{v} \times \vec{B}) dt.$$

Using $\vec{v} = \frac{\vec{P}}{\gamma m_0}$,

$$d\vec{P} = \frac{q}{\gamma m_0} (\vec{P} \times \vec{B}) dt.$$

The simulation calculates in steps of distance instead of time. Therefore a conversion of dt is necessary

$$dt = \frac{ds}{v}.$$

For (ultra) high energy cosmic rays $v \approx c$,

$$d\vec{P} = \frac{q}{\gamma m_0} (\vec{P} \times \vec{B}) \frac{ds}{c}.$$

And for the same reason the mass can be neglected with respect to the energy and momentum $\gamma = \frac{E}{m_0 c^2} \approx \frac{Pc}{m_0 c^2}$ resulting in,

$$d\vec{P} = \frac{q}{P} (\vec{P} \times \vec{B}) ds.$$

Now change units to eV

$$\begin{aligned} d\vec{P} &= \frac{qc}{e \cdot P} (\vec{P} \times \vec{B}) ds, \\ &= \frac{Zc}{P} (\vec{P} \times \vec{B}) ds. \end{aligned}$$

D

APPENDIX D

Bending radius of a charged particle in a magnetic field, the easy way.

To check if the program works correctly the radius of curvature due to a magnetic field can be calculated. A simple non-relativistic example is used, were \vec{v} is perpendicular to \vec{B} . Setting the centripetal force equal to the Lorentz force results in

$$\begin{aligned}\frac{mv^2}{r} &= Bqv, \\ \frac{mv}{r} &= Bq, \\ r &= \frac{P}{qB},\end{aligned}$$

with $P = mv$.

Change units to eV

$$\begin{aligned}r &= \frac{Pe}{qcB}, \\ &= \frac{P [eV]}{ZcB}.\end{aligned}$$

Change radius of curvature to astronomical units

$$\begin{aligned}r[\text{AU}] &= \frac{1}{1.5 \cdot 10^{11} \cdot c} \frac{P [eV]}{Z \cdot B}, \\ &= \frac{1}{4.5 \cdot 10^{19}} \frac{P [eV]}{Z \cdot B [\text{T}]}. \end{aligned}$$

BIBLIOGRAPHY

- [1] N.M. Gerasimova and G.T. Zatsepin, *Splitting of cosmic ray nuclei by solar photons*, Soviet Phys., JETP, vol. 11, 899, 1960.
- [2] G. A. Medina-Tanco and A. A. Watson, *The photodisintegration of cosmic ray nuclei by solar photons: The Gerasimova-Zatsepin effect revisited*, Astropart. Phys. 10, 157–164, 1999.
- [3] J. Wouda, *Simulation of the Gerasimova-Zatsepin effect for HiSPARC*, 2013.
- [4] B. de Gier, *Prospects of measuring Gerasimova-Zatsepin events using the HiSPARC network*, 2013.
- [5] L. N. Epele, S. Mollerach and E. Roulet, *On the disintegration of cosmic ray nuclei by solar photons*, 1999.
- [6] A. Iyono, et al. (LAAS collaboration), *Cosmic ray composition studies through the Gerasimova-Zatsepin effects of heavy nuclei at LAAS*, Astrophys. Space Sci. Trans., 7, 327-333, 2011.
- [7] S. Lafèbre, H. Falcke, J. Hörandel, J. Kuijpers, *Prospects for direct cosmic ray mass measurements through the Gerasimova-Zatsepin effect*, A & A 485, 1-4, 2008.
- [8] M. Planck, *Zur theorie des Gesetzes der Energieverteilung im Normalspectrum*, Verhandlungen der deutsche physikalischen Gesekkschaft im Jahre 1900, Jahrg. 2, Nr. 17, 237-245, 1900.
- [9] J. Stefan, *Über die Beziehung zwischen der Wärmestrahlung und der Temperatur*, Sitzungsberichte der Mathematisch-naturwissenschaftlichen Classe der kaiserlichen Akademie der Wissenschaften 79, 391-428, 1879.
- [10] L. Boltzmann, *Ableitung des Stefan'schen Gesetzes, betreffend die Abhängigkeit der Wärmestrahlung von der Temperatur aus der elektromagnetischen Lichttheorie*, Annalen der Physik und Chemie 258 (6), 291-294, 1884.
- [11] J.H. Lambert, *Photometria, sive de Mensura et gradibus luminis, colorum et umbrae*, Augsburg, Christoph Peter Detleffsen for the widow of Eberhard Keltt, 1760.
- [12] G. Kopp and J.L. Lean, *A new, lower value of total solar irradiance: Evidence and climate significance*, Geophysical Research Letters (2011) 38.

- [13] F. W. Stecker, *Photodisintegration of Ultrahigh Energy Cosmic Rays: A New Determination*, *Astrophys.J.*, 512, 1999.
- [14] J. L. Puget, F. W. Stecker and J. H. Bredekamp, *Photonuclear interactions of ultrahigh energy cosmic rays and their astrophysical consequences*, *Astropart.Phys.J.*, 205:638–654237, 1976.
- [15] A. I. Akasofu, P. C. Gray and L. C. Lee, *A model of the heliospheric magnetic field configuration*, 1979.
- [16] Y. M. Wang and N. R. Sheeley,Jr, *Modeling the sun's large-scale magnetic field during the maunder minimum*, *Astrophys.J.*, 591:1248–1256, 2003 July 10.
- [17] M. Nagano and A.A. Watson, *Observations and implications of the ultrahigh-energy cosmic rays*, *Rev. of Modern Phys.*, Vol. 72, No. 3, July 2000.
- [18] Pictures taken from auger.org.
- [19] D. B. R. A. Fokkema, *The HiSPARC Experiment, data acquisition and reconstruction of shower direction*, ISBN: 978-90-365-3438-3 DOI: 10.3990/1.9789036534383, 2012.
- [20] Pictures taken from hisparc.nl.
- [21] The Auger Collaboration, *Pierre Auger project design report*, www.auger.org , October 31st 1995.
- [22] A. Jonqui  re, *Not sur la s  rie $\sum_{n=1}^{\infty}$* , *Bulletin de la Soci  t   Math  matique de France*, 17, 142-152, 1889.

ACKNOWLEDGEMENTS

I learned a lot! But it wasn't possible without a number of people. Therefore I thank my family and friends for their interest and support during my study. I thank Prof. Dr. S.J. de Jong for realizing the possibility to do a research master. I admire his knowledge and ambition to improve the Dutch educational system. I thank Dr. C.W.J.P. Timmermans for supervising this master thesis. I enjoyed working together, enlightened by our shared sense of humor. I thank my fellow students. I enjoyed spending time with you for discussions, lunch, coffee breaks and occasionally a beer or two. I thank my high school for their cooperation and my colleagues for their flexibility during the sometimes busy periods. I thank my graduation students, teaching them was a nice variation while researching.

Nijmegen, July 2015

J.V.R. van Eijden